

## Review

**Cite this article:** Su T-E, Chen Y-X, Huang T-W, Chien Y-H and Yu B-Y (2025). Current progress, potentials, and challenges for developing photo-assisted CO<sub>2</sub> conversion processes. *Cambridge Prisms: Carbon Technologies*, **1**, e7, 1–20 <https://doi.org/10.1017/cat.2025.10008>

Received: 15 April 2025

Revised: 04 November 2025

Accepted: 10 November 2025

### Keywords:


CO<sub>2</sub> utilization; photoreduction; photothermal catalyst; process development; decarbonization; process modeling

**Corresponding authors:** Bor-Yih Yu and Yi-Hsin Chien;

Emails: [boryihyu@ntu.edu.tw](mailto:boryihyu@ntu.edu.tw); [yhchien@fcu.edu.tw](mailto:yhchien@fcu.edu.tw)

T-E.S., Y-X.C. and T-W.H. are contributed equally.

# Current progress, potentials, and challenges for developing photo-assisted CO<sub>2</sub> conversion processes

Ting-En Su<sup>1</sup>, Yu-Xuan Chen<sup>1</sup>, Ting-Wei Huang<sup>2</sup>, Yi-Hsin Chien<sup>1</sup> and Bor-Yih Yu<sup>2</sup> 

<sup>1</sup>Materials Science and Engineering, Feng Chia University, Taiwan and <sup>2</sup>Chemical Engineering, National Taiwan University, Taiwan

## Abstract

The utilization of carbon dioxide (CO<sub>2</sub>) has garnered significant attention as a strategy to mitigate anthropogenic emissions. Within this field, the conversion processes of CO<sub>2</sub> through photocatalytic systems have emerged as a particularly noteworthy area of research. This approach leverages solar energy for the reaction and is considered a promising and environmentally friendly alternative to traditional thermally driven catalytic systems. This article aims to summarize recent advancements in several key photo-conversion pathways, including the synthesis of methane, methanol, C<sub>2</sub> hydrocarbons, dimethyl carbonate, and glycerol carbonate. Additionally, potential configurations for the development of processes aimed at producing various chemicals will be proposed. Current insights indicate that the photocatalytic conversion of CO<sub>2</sub> could be effectively integrated with chemical absorption methods, provided that appropriate separation and process intensification strategies are developed. From an economic perspective, the photocatalytic reduction of CO<sub>2</sub> minimizes the reliance on green hydrogen as a hydrogen source, thereby significantly improving overall economic viability. Environmentally, it is essential to enhance the reaction conversion and product selectivity of the photocatalytic conversion processes to maximize their decarbonization potential. Overall, this paper is particularly suited for readers who are new to this field and are interested in transitioning from experimental work to process development.

## Impact statement

This review paper discusses recent advancements in the field of photocatalytic CO<sub>2</sub> conversion. It covers the fundamentals and key materials used in photocatalysis, various conversion pathways for producing both commodity and value-added chemicals, and potential process configurations based on the current understanding of existing technologies. Key points for enhancing economic and environmental performance are also provided. This paper will be beneficial for readers who are new to this field and are interested in transitioning from experimental work to process development.

## Introduction

Photocatalytic reaction technologies have emerged as a significant area of research in CO<sub>2</sub> utilization. It harnesses solar energy to drive the transformation of carbon dioxide into value-added fuels and chemicals under mild conditions. Traditionally, CO<sub>2</sub> conversion has been carried out using thermal catalytic methods. This conversion can be classified as either non-reductive or reductive, depending on whether the oxidation state of the carbon atom changes during the reaction. Reductive conversion primarily refers to the hydrogenation of CO<sub>2</sub> to form hydrocarbons, alcohols, and others. In contrast, non-reductive pathways convert CO<sub>2</sub> directly into various classes of chemicals, including alkyl carbonates (which react with alcohols), aliphatic polycarbonates (which react with diols), ureas (which react with amines), and carbamates (which react with both alcohols and amines) (Tomishige et al., 2019; Tomishige et al., 2020). Table 1 summarizes some pathways that have been widely reported in the literature. However, thermal catalytic conversion of CO<sub>2</sub> has several drawbacks, including the requirement for elevated temperatures and pressures and challenges related to CO<sub>2</sub> activation. In contrast, photocatalytic CO<sub>2</sub> conversion, driven by solar energy and operating under milder conditions, inherently offers greater sustainability compared to thermal catalytic systems.

Overall, photocatalytic reactions utilize photon energy to generate charge carriers that directly drive CO<sub>2</sub> reduction under relatively mild conditions (Guo et al., 2023). Conventional photocatalytic reactions rely on the electron–hole pairs upon light irradiation (typically UV or visible lights), which enables redox reactions involving CO<sub>2</sub> and co-reactants. Materials with appropriate bandgaps (e.g., the semiconductor type) have been extensively investigated as the catalysts.

© The Author(s), 2025. Published by Cambridge University Press. This is an Open Access article, distributed under the terms of the Creative Commons Attribution licence (<http://creativecommons.org/licenses/by/4.0>), which permits unrestricted re-use, distribution and reproduction, provided the original article is properly cited.

 Cambridge Prisms

 CAMBRIDGE UNIVERSITY PRESS

**Table 1.** Possible reaction pathways for CO<sub>2</sub> conversion

Entry	Products	Thermal catalytic conversion			Photo-assisted conversion
		Co-reactant	Catalyst	Process Design	
1	CO	Hydrogen (R)	(Liu et al., 2022; Wang et al., 2023)	(Cao et al., 2022)	(Wu et al., 2023; Liang et al., 2023)
2	Methane	Hydrogen (R)	(Summa et al., 2022; Lin et al., 2021)	(Uddin et al., 2022)	(Yang et al., 2022; Omr et al., 2023)
3	Ethylene	Hydrogen (R)	-	(Chiu & Yu, 2024a,b)	(Asiri et al., 2025; Wang et al., 2025)
4	Methanol	Hydrogen (R)	(Quilis et al., 2023; Onishi & Himeda, 2022)	(Lin et al., 2024; Chiou et al., 2023)	(Xu et al., 2023; Xie et al., 2020)
5	Ethanol	Hydrogen (R)	(Lou et al., 2021; Wang et al., 2021)	(He et al., 2023)	(Yu et al., 2022; Das et al., 2023)
6	Propanol	Hydrogen (R)	(Ahlers et al., 2014; Lage et al., 2023)	(Lee et al., 2025; Vo et al., 2022)	-
7	Formic acid	Hydrogen (R)	(Mori et al., 2020; Weilhard et al., 2021)	(Pérez-Fortes et al., 2016)	(He et al., 2023; Wang et al., 2022)
8	Fischer-Tropsch Fuels	Hydrogen (R)	(Gong et al., 2020; Wang et al., 2022)	(Jhuang et al., 2025)	-
9	Dimethyl carbonate	Ethylene oxide/methanol (IND)	(Wang et al., 2014; Deng et al., 2020)	(Yu et al., 2018; Ramezani et al., 2020)	-
		Methanol (NR)	(Jiang et al., 2023; Chaban et al., 2024)	(Lee et al., 2021)	(Jin et al., 2023; Guan et al., 2024)
10	Diethyl carbonate	Ethanol (NR)	(Putro et al., 2024; Putro et al., 2022)	(Yu et al., 2020)	-
11	Dipropyl carbonate	Propanol (NR)	(Ma et al., 2013)	(Lee et al., 2021)	-
12	Dibenzyl carbonate	Benzyl alcohol (NR)	(Fiorani & Selva, 2014)	-	-
13	Glycerol carbonate	Glycerol (NR)	(Alassmy et al., 2021; Hu et al., 2021)	-	(Li et al., 2021; Liu et al., 2022)
		Propylene oxide/glycerol (IND)	(Alassmy et al., 2021; Luo et al., 2024)	(Wu et al., 2024)	-
14	Isopropyl n-phenyl carbamate	Isopropyl alcohol/Phenyl aniline (NR)	(Gu et al., 2023)	(Lee et al., 2021; Huang et al., 2023)	-
15	Poly (butylene carbonate)	1,4-butanediol (NR)	(Hu et al., 2018; Tu et al., 2023)	(Yu et al., 2020)	-
16	Urea	Methyl amine (NR)	(Yabushita et al., 2024; More & Srivastava, 2021)	(Zhang et al., 2021)	(Yang et al., 2023; Ahmad et al., 2025)

Existing examples include converting CO<sub>2</sub> to CO (Chu et al., 2022; Liao et al., 2024), methane (Lee et al., 2021; Zhao et al., 2024), methanol (Xi et al., 2022; Huang et al., 2024), and C<sub>2+</sub> hydrocarbons (Song et al., 2024; Zhang et al., 2024). However, such processes are currently limited by low conversion and selectivity due to inefficient CO<sub>2</sub> adsorption and activation, rapid recombination of charge carriers, limited visible-light absorption, and insufficient catalyst stability. More recently, photothermal CO<sub>2</sub> conversion has emerged as a novel technology (Gao et al., 2020). It integrates light-induced excitation with thermal activation to enhance catalytic performance (Gao et al., 2020). Under solar or near-infrared irradiation, localized heating and energetic carriers promote charge separation, accelerate diffusion, and expand the usable solar spectrum (Cai et al., 2021). Materials exhibiting plasmonic properties or broad-spectrum absorption have been reported as effective catalysts for photothermal conversion. In addition to producing chemicals similar to those from conventional photocatalytic systems (Cai et al., 2021; Wu et al., 2021; Li et al., 2022; Deng et al., 2023), photothermal systems can also convert CO<sub>2</sub> into larger molecules such as dimethyl carbonate

(DMC) (Jin et al., 2023) or glycerol carbonates (GC) (Li et al., 2024). Although photothermal catalysis demonstrates improved conversion efficiency, it still faces challenges such as the need for elevated temperatures and pressures, and concerns over long-term catalyst stability (Gao et al., 2020).

Recent landmark reviews have advanced the understanding of photocatalytic CO<sub>2</sub> conversion. For instance, Fang *et al.* provided a comprehensive overview of catalyst synthesis, reactor design, testing protocols, and mechanistic studies (Fang et al., 2023). Sadanandan *et al.* highlighted efficiency limitations due to charge-carrier recombination and narrow visible-light absorption, and proposed strategies to address them (Sadanandan et al., 2024). Kumar *et al.* investigate multifunctional carbon-nitride nano-architectures, demonstrating how bandgap tuning and surface-site control enable both hydrogen evolution and CO<sub>2</sub> reduction (Kumar et al., 2023). Gao et al. compared photocatalytic and photothermal CO<sub>2</sub> conversion as promising routes for CO<sub>2</sub> utilization, detailing their principles, catalyst options, and performance metrics (Gao et al., 2020). Overall, this field remains emerging, with many aspects yet to be explored.

Extensive research has advanced both theoretical and experimental aspects of photocatalytic CO<sub>2</sub> conversion, yet gaps remain between lab-scale studies and process development. The absence of integrated frameworks for process studies limits discussion of economic, environmental, and safety considerations. Currently, the low product yields and selectivity of photocatalytic CO<sub>2</sub> conversion hinders its practical deployment, highlighting the importance downstream separation strategies. To address this gap, this review aims to provide insights for advancing from experimentation to process development. It begins by summarizing advances in photocatalyst design, particularly focusing on the incorporation of heterojunction architectures, surface defect engineering, active site optimization, and enhanced reaction capacities to enable the efficient conversion of CO<sub>2</sub> into valuable hydrocarbon fuels. Subsequently, essential perspectives for further advancing photocatalytic CO<sub>2</sub> conversion processes are presented. Overall, this review offers readers a comprehensive framework that connects material fundamentals to plant-wide process implementation.

## State-of-the-art progress in photocatalytic conversion of CO<sub>2</sub>

This section reviews recent advancements in the field. Section “Introduction of photocatalytic conversion” introduces potential photocatalysts for CO<sub>2</sub> conversion. Sections “Photocatalytic reduction systems” and “Photothermal catalytic reaction systems” summarize recent experimental results on photocatalytic reduction and photothermal catalytic systems, respectively. Section “Standard procedure of photocatalytic CO<sub>2</sub> conversion” covers standardized procedures for experimentation and process development, while Section “Modeling” highlights recent progress in modeling photocatalytic reaction systems.

### Introduction of photocatalytic conversion

#### Fundamentals of photocatalytic conversion

Photocatalysis involves three key stages: light absorption, charge carrier generation and separation, and surface redox reactions (Du et al., 2020). Upon photon excitation, electrons (e<sup>−</sup>) are promoted from the valence band (VB) to the conduction band (CB), resulting in the formation of holes (h<sup>+</sup>) that drive reduction and oxidation reactions, including CO<sub>2</sub> conversion and pollutant degradation under ambient conditions. Accordingly, the overall efficiency (η<sub>e</sub>) of a photocatalytic system can be represented by **Equation (1)** (Li et al., 2015):

$$\eta_e = \eta_a \times \eta_{ce} \times \eta_{cs} \times \eta_{cu} \quad (\text{Eq1})$$

Where η<sub>a</sub> denotes the photon absorption efficiency, η<sub>ce</sub> represents the charge excitation efficiency, η<sub>cs</sub> refers to the efficiency of charge separation and transport, and η<sub>cu</sub> indicates the efficiency of charge carrier utilization in surface reactions (Zhang et al., 2021). Optimizing light harvesting (η<sub>a</sub>) is critical, as it directly influences both η<sub>ce</sub> and η<sub>cs</sub>. Strategies to enhance photocatalytic efficiency include tuning the bandgap, crystal structure, and surface area. The development of composite materials with extended spectral absorption ranges (UV–VIS–NIR), engineered heterojunctions, defect-engineered nanostructures, and integration of co-catalysts has been shown to improve charge separation and increase the density of active sites (Li et al., 2021; Man et al., 2024; Li et al., 2016).

#### Potential photocatalyst design strategies

Conventional semiconductor metal oxides remain prevalent in photocatalytic applications due to their ability to facilitate UV-driven

charge separation between the VB and CB. Nevertheless, their broad band gaps and limited electrical conductivity restrict their effectiveness in solar energy applications, considering that ultraviolet light accounts for merely about 5% of the solar spectrum. To exploit visible and infrared light, whereas the light accounts for approximately 46% and 49%, two-dimensional (2D) materials such as carbon-based substances (e.g., graphene and graphitic carbon nitride, g-C<sub>3</sub>N<sub>4</sub>), transition metal dichalcogenides (TMDs), and MXenes have emerged as promising alternatives. These materials exhibit tunable band gaps that can be aligned with the conduction and valence bands to match the reduction potential of CO<sub>2</sub> and the corresponding oxidation half-reactions. Elemental doping or substitution techniques have been employed to modulate the bandgap and Fermi level, thereby positioning the conduction band minimum (CBM) just above the CO<sub>2</sub>/CO or CO<sub>2</sub>/CH<sub>4</sub> reduction potentials (Lee et al., 2021; Li et al., 2024; Huang et al., 2025).

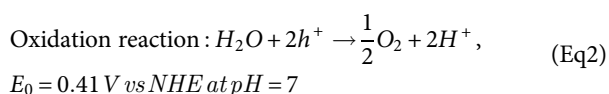
Furthermore, TMDs and MXenes have attracted considerable interest owing to their abundant surface atoms and compatibility with co-catalysts. Representative TMDs, including MoS<sub>2</sub>, WS<sub>2</sub>, ReS<sub>2</sub>, and NiS<sub>2</sub>, whereas MXenes are generally described by the formula M<sub>n</sub>+<sub>1</sub>X<sub>n</sub>T<sub>x</sub>, where M denotes transition metals such as Ti, V, or Nb; X represents carbon and/or nitrogen; and T corresponds to surface terminations like -O, -OH, or -F. These materials possess metallic conductivity, high surface reactivity, adaptable electronic structures, and strong interactions with co-catalysts, rendering them suitable for solar-driven CO<sub>2</sub> conversion (Kuang et al., 2020). Heterostructure engineering approaches—including Type-II heterojunctions, Z-scheme architectures, core-shell structures, and 2D/2D or 2D/0D systems—offer ultrathin, layered configurations that minimize charge carrier diffusion distances and suppress electron–hole recombination, thereby enhancing photocatalytic performance (Zeng et al., 2020; Xu et al., 2018; Wang et al., 2018; Cai et al., 2024; Wang et al., 2021). Defect engineering introduces localized electronic states that serve as active sites for CO<sub>2</sub> adsorption and activation, while also modulating charge carrier dynamics. The presence of oxygen vacancies, cation vacancies, and other point defects can enhance CO<sub>2</sub> adsorption and stabilize reaction intermediates (Vennapoosa et al., 2023; Wang et al., 2021; Ji et al., 2023).

Porous crystalline materials, including metal–organic frameworks (MOFs) and covalent organic frameworks (COFs), also demonstrate potential due to their high surface areas and ordered pore structure that facilitate CO<sub>2</sub> capture and activation (Chemical Reviews, 2012). However, their low electrical conductivity and rapid charge recombination limit performance. Recent research has improved these issues by hybridizing them with conductive materials and incorporating co-catalyst systems to enhance charge transport and visible-light responsiveness (Altintas et al., 2022).

In summary, advanced photocatalysts, ranging from metal oxides and 2D nanostructures to porous frameworks, enable efficient CO<sub>2</sub> conversion into value-added products such as methane, methanol, ethylene, and ethanol. Continued innovations in material design, interface engineering, and mechanistic understanding will be essential to fully realize the potential of photocatalytic CO<sub>2</sub> reduction.

### Photocatalytic reduction systems

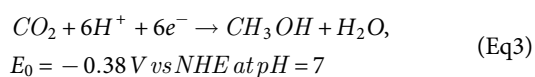
Among various pathways, photocatalytic CO<sub>2</sub> reduction that produces C<sub>1</sub> and C<sub>2</sub> chemicals has been the primary focus of this field. Typically, the hydrogen source for these reactions is derived from water splitting, as illustrated in **Equation (2)**.



This reaction is combined with the multi-electron reduction of CO<sub>2</sub> to produce the targeted chemicals. Table 2 provides a comparative overview of representative photocatalytic reduction pathways, highlighting their compositional features, corresponding CO<sub>2</sub> reduction products, and associated product selectivity. The following sections will discuss the advancements in producing C<sub>1</sub> products (e.g., methanol and methane) and C<sub>2</sub> products (e.g., ethane and ethylene) via photocatalytic CO<sub>2</sub> reductive pathways.

### Production of methanol

Methanol is a primary focus in the domain of CO<sub>2</sub> utilization due to its multifunctional role as an energy storage medium, a sustainable fuel alternative, and a precursor for the synthesis of diverse hydrocarbons. The photocatalytic conversion of CO<sub>2</sub> to MeOH entails a six-electron reduction mechanism, as described by the standard reaction depicted in Equation (3):

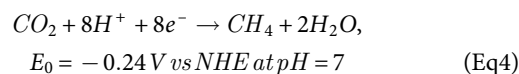


Notably, the reduction potential of this reaction is slightly more positive than that of proton reduction (−0.41 V vs NHE), making it thermodynamically favorable under photocatalytic conditions. However, achieving efficient methanol production requires prolonged lifetimes of photoinduced charge carriers and effective charge separation. To this end, heterojunction engineering through metal or metal oxide modification of semiconductor photocatalysts has significantly improved charge carrier dynamics. For instance, Zhang *et al.* reported a vertically oriented Fe single-atom-decorated TiO<sub>2</sub>/SrTiO<sub>3</sub> nanotube heterojunction (Fe-TSr), which enables directional separation and migration of photogenerated carriers. This system achieved a methanol yield of 154.20 μmol·g<sub>cat</sub><sup>−1</sup>·h<sup>−1</sup> with 98.90% selectivity in pure water, representing 50- and 3-fold enhancements relative to pristine TiO<sub>2</sub> and TSr, respectively (Huang *et al.*, 2024). Similarly, Ag-doped 2H-MoS<sub>2</sub> composites have shown promising performance in CO<sub>2</sub> photoreduction. The incorporation of 20 wt% Ag resulted in the highest methanol yield of 365.08 μmol·g<sub>cat</sub><sup>−1</sup>·h<sup>−1</sup>. This improvement is attributed to the formation of a Schottky barrier at the Ag-MoS<sub>2</sub> interface, facilitating efficient electron transfer from the conduction band of MoS<sub>2</sub> to Ag nanoparticles, while photogenerated holes participate in the oxidation of C<sub>3</sub>H<sub>8</sub>O to C<sub>3</sub>H<sub>6</sub>O. Thus, the barrier effectively suppresses charge recombination and prolongs carrier lifetimes (Zheng *et al.*, 2019). Furthermore, enhancing CO<sub>2</sub> adsorption and activation is vital for improving methanol production rates and selectivity. Li and co-workers developed a ternary heterostructure comprising 2.5% g-C<sub>3</sub>N<sub>4</sub>/1% CuO@MIL-125(Ti). In this system, MIL-125(Ti) offers a high surface area and porosity, CuO quantum dots facilitate CO<sub>2</sub> capture and activation, and g-C<sub>3</sub>N<sub>4</sub> nanosheets provide efficient charge transport pathways. Mott-Schottky analysis revealed that electrons and holes are spatially separated across the conduction band of CuO and the valence band of g-C<sub>3</sub>N<sub>4</sub>, respectively, reducing recombination losses. The composite photocatalyst exhibited high activity, yielding CO (180.1 μmol/g), CH<sub>3</sub>OH (997.2 μmol/g), CH<sub>3</sub>CHO (531.5 μmol/g), and CH<sub>3</sub>CH<sub>2</sub>OH (1505.7 μmol/g) using water as the electron donor (Li *et al.*, 2020).

### Production of methane

Methane (CH<sub>4</sub>) serves not only as a clean and efficient fuel but also as a valuable intermediate for synthesizing syngas, hydrogen, and

methanol through reforming processes. Among various C<sub>1</sub> products derived from CO<sub>2</sub> reduction, methane formation requires the highest number of electrons (eight) but has the least negative reduction potential. The thermodynamic stability of CO<sub>2</sub>, characterized by a high C=O bond dissociation energy (~750 kJ/mol), necessitates a high density of electrons and protons to drive its conversion into CH<sub>4</sub>. This reaction follows an eight-electron reduction pathway, as illustrated in Equation (4) (Yang *et al.*, 2023):



Among the proposed mechanisms, the carbene pathway is considered more plausible than the formaldehyde pathway. The rate-determining step is the protonation of adsorbed CO (\*CO) to form \*CHO, followed by further hydrogenation steps to \*CHOH, \*CH, \*CH<sub>2</sub>, \*CH<sub>3</sub>, and ultimately CH<sub>4</sub>. To promote this multi-electron transfer process, constructing an electron-rich micro-environment around the catalytic sites is essential. Strategies include incorporating plasmonic noble metal nanoparticles (Yan *et al.*, 2024) and π-conjugated systems such as COFs or 2D materials (Wang *et al.*, 2018; Madi & Tahir, 2024), which enhance charge mobility and surface area. Liu *et al.* introduced a BiVO<sub>4</sub>@-TiO<sub>2</sub> nanograin/needle array (NNAs) S-scheme heterojunction photocatalyst, further modified with 5 wt% of the ionic liquid 1-butyl-3-methylimidazolium tetrafluoroborate (BMIM-BF<sub>4</sub>) to improve CO<sub>2</sub> solubility in aqueous systems. Under Xe lamp irradiation, photo-induced electrons from BiVO<sub>4</sub> and holes from TiO<sub>2</sub> undergo rapid recombination at the interface, resulting in electron accumulation at the TiO<sub>2</sub> tip and hole enrichment in BiVO<sub>4</sub>. This charge spatial separation significantly enhances the photocatalytic performance, achieving CO, CH<sub>4</sub>, and H<sub>2</sub> evolution rates of 321.5, 132.7, and 75.8 μmol·m<sup>−2</sup>·h<sup>−1</sup>, respectively (Zhao *et al.*, 2024). Moreover, Shankar *et al.* demonstrated a plasmonic photonic crystal photocatalyst comprising Au nanoparticle-decorated, periodically modulated TiO<sub>2</sub> nanotube arrays (Au-PMTiNTs). The Z-scheme heterojunction, enhanced by hot-electron transfer under AM1.5G simulated sunlight, selectively produced CH<sub>4</sub> at 302 μmol·g<sub>cat</sub><sup>−1</sup>·h<sup>−1</sup> with 89.3% selectivity (Zeng *et al.*, 2020). COFs have also emerged as promising platforms for CO<sub>2</sub> photoreduction due to their tunable molecular structures, adjustable band gaps, and efficient internal charge transport. Maji and co-worker synthesized a triazole-linked COF (TFPB-TRZ) that delivered a remarkable CH<sub>4</sub> production rate of 61.62 mmol·g<sub>cat</sub><sup>−1</sup>·h<sup>−1</sup> with an overall yield of 493 mmol·g<sup>−1</sup> and excellent selectivity (~99%) under visible-light irradiation. *In situ* diffuse reflectance infrared Fourier transform spectroscopy (DRIFTS) confirmed the formation of key intermediates such as \*COOH, \*CO, \*CH<sub>2</sub>O, \*CH<sub>3</sub>O, -CH<sub>2</sub>, and -CH<sub>3</sub>, substantiating the eight-electron reduction pathway leading to methane formation (Biswas *et al.*, 2024).

### Production of ethylene

The production of C<sub>2</sub><sup>+</sup> hydrocarbons, particularly ethylene (C<sub>2</sub>H<sub>4</sub>) and acetylene (C<sub>2</sub>H<sub>2</sub>), through photocatalytic reduction is of special interest due to their high energy densities and essential roles as industrial feedstocks. However, the conversion is hindered by CO<sub>2</sub>'s high thermodynamic stability (bond dissociation energy ~750 kJ/mol; ΔG°<sub>298K</sub> = −394.36 kJ/mol). Efficient C-C bond formation, typically achieved through the dimerization of C<sub>1</sub> intermediates (e.g., CH<sub>2</sub>, CH<sub>3</sub>, or CHO), is crucial for synthesizing C<sub>2</sub> products. These multistep, multi-electron/proton processes require surfaces with high charge carrier and proton densities, as well as strong adsorption of intermediates to avoid premature desorption



Table 2. The comparison of various catalytic systems

Product	Type	Materials type	Photocatalyst	Operating parameter	Light source	CO <sub>2</sub> feeding conditions	Yield ( $\mu\text{mol}\cdot\text{g}^{-1}\cdot\text{h}^{-1}$ )	Selectivity (%)	Ref
Methane	Photo-thermal	Metal oxides	N-doped CD/TOH	T = 80 °C P = 1 bar V = 80 mL	Xe arc lamp (300 W)	CO <sub>2</sub> gas with an interior pressure of ~1 bar	26.8	98	(Lee et al., 2021)
			BiVO <sub>4</sub> @TiO <sub>2</sub> NNAs	T = ambient P = 1.013 bar V = 110 mL	Xe lamp (300 W)	High-purity CO <sub>2</sub> gas with 5% BMIM-BF <sub>4</sub>	132.7 ( $\mu\text{mol}\cdot\text{m}^{-2}\cdot\text{h}^{-1}$ )	57.3	(Zhao et al., 2024)
			Au@ZnS/3D-M-mTiO <sub>2</sub>	T = 20 °C	Xe lamp (300 W) ( $\lambda = 320\text{--}780\text{ nm}$ )	0.1 MPa CO <sub>2</sub> pressure	33.2	91.5	(Li et al., 2024)
			Pd NPs/TiO <sub>2</sub>	T = 35–60 °C V = 48 cm <sup>3</sup>	Xe lamp (600 W/m <sup>2</sup> ) AM 1.5G filter	Pure CO <sub>2</sub> (99%), 0.25 MPa	30.7	95.29	(Huang et al., 2025)
			Au-PMTINTs	T < 80 °C P = 50 psi CO <sub>2</sub> V = 48 cm <sup>3</sup>	AM 1.5 G Solar simulator (100 mW/cm <sup>2</sup> )	CO <sub>2</sub> pressure, 50 psi	302	89.3	(Zeng et al., 2020)
			N-doping CeO <sub>2</sub> -AH FLPs	T = 25 °C V = 100 mL	Xe lamp (500 mW/cm <sup>2</sup> )	CO <sub>2</sub> (99.99%)	35.35	17.69	(Yan et al., 2024)
			Pd-CeO <sub>2</sub>	P = 1.013 bar	Xe lamp (100 mW/cm <sup>2</sup> ) AM1.5G filter	High-purity CO <sub>2</sub> at atmospheric pressure	41.6	99	(Wang et al., 2022)
			AuAg-CeO <sub>2</sub>	-	Xe lamp (300 W) AM1.5G filter	1.5 g of NaHCO <sub>3</sub> , 10 mL of H <sub>2</sub> SO <sub>4</sub> (0.78 mol/L) in pure CO <sub>2</sub> (l)	30.87	94.5	(Yan et al., 2024)
			S-C/In <sub>2</sub> O <sub>3</sub> -CeO <sub>2</sub>	T = 25 °C P = 1.013 bar V = 80 mL	Xe lamp (100 mW/cm <sup>2</sup> ) AM1.5G filter	CO <sub>2</sub> gas (99.999%) in DI at ambient pressure	60.6	92.4	(Wang et al., 2021)
			Pt/Au-CeO <sub>2</sub>	-	Xe lamp (4000 mW/cm <sup>2</sup> ) AM1.5 filter	1% CO <sub>2</sub> and 99% N <sub>2</sub> and 1 mL of DI water	369.4	97.6	(Ren et al., 2024)
			Ru-TiO <sub>x</sub>	T = 276 °C V = 300 mL	Xe lamp (300 W)	20% CO <sub>2</sub> and 80% H <sub>2</sub> for 30 min purged	22.35 ( $\text{mmol}\cdot\text{g}^{-1}\cdot\text{h}^{-1}$ )	99.99	(Dong et al., 2023)
			Ru/MnO/Mn <sub>3</sub> O <sub>4</sub>	T = 200 °C P = 1 MPa V = 180 mL	Xe lamp (300 W)	20% CO <sub>2</sub> and 80% H <sub>2</sub> purged with 10 mL water	166.7 ( $\text{mmol}\cdot\text{g}^{-1}\cdot\text{h}^{-1}$ )	99.5	(Zhai et al., 2024)
			Ru/MnCo <sub>2</sub> O <sub>4</sub>	T = 150–230 °C P = 1.013 bar (flow) GHSV = 24,000 mL·h <sup>-1</sup> ·gcat <sup>-1</sup>	Xe lamp (300 W)	CO <sub>2</sub> :H <sub>2</sub> = 1:4	66.3 ( $\text{mmol}\cdot\text{g}^{-1}\cdot\text{h}^{-1}$ )	96.0	(Guo et al., 2023)
			Ru <sub>x</sub> Co <sub>1-x</sub> /TiO <sub>2</sub>	T = 150–230 °C P = 1.013 bar (flow) GHSV = 24,000 mL·h <sup>-1</sup> ·gcat <sup>-1</sup>	Xe lamp (300 W)	CO <sub>2</sub> :H <sub>2</sub> = 1:4	191.0	94.6	(Tang et al., 2024)

(Continued)

Table 2. (Continued)

Product	Type	Materials type	Photocatalyst	Operating parameter	Light source	CO <sub>2</sub> feeding conditions	Yield ( $\mu\text{mol}\cdot\text{g}^{-1}\cdot\text{h}^{-1}$ )	Selectivity (%)	Ref
	MXene		$\text{Ru}_x\text{Ni}_{1-x}/\text{TiO}_2$	T = 100–310 °C P = 1.013 bar (flow) GHSV = 24,000 mL·h <sup>-1</sup> ·gcat <sup>-1</sup> ( $\lambda$ = 200–1100 nm)	Xe lamp (300 W, 1.8 W/cm <sup>2</sup> ) ( $\lambda$ = 200–1100 nm)	CO <sub>2</sub> :H <sub>2</sub> = 1:4	3.58 ( $\text{mol}\cdot\text{g}^{-1}\cdot\text{h}^{-1}$ )	94.0	(Guo et al., 2025)
			xCo/CeO <sub>2</sub>	T = 150–450 °C P = 1.013 bar (flow) GHSV = 12,000 mL·h <sup>-1</sup> ·gcat <sup>-1</sup>	White LED (2.0 + 0.1 W/cm <sup>2</sup> ) ( $\lambda$ = 420–710 nm)	N <sub>2</sub> :CO <sub>2</sub> :H <sub>2</sub> = 1:1:4	<55% (CO <sub>2</sub> conversion)	-	(OConnell et al., 2024)
			Ni/Nb <sub>2</sub> C	T = 150–400 °C P = 1.013 bar (batch/flow)	Xe arc lamp (300 W)	CO <sub>2</sub> :H <sub>2</sub> = 1:1	83.4 ( $\text{mmol}\cdot\text{g}^{-1}\cdot\text{h}^{-1}$ )	80.9	(Wu et al., 2021)
	Photo-Carbonaceous	CuPc/g-C <sub>3</sub> N <sub>4</sub>	V = 200 mL	Xe lamp (300 W) AM1.5G filter	99.99% CO <sub>2</sub> gas	39.8	90	(Chen et al., 2025)	
		SnS/g-C <sub>3</sub> N <sub>4</sub>	T = ambient P = 1.013 bar V = 25 mL	Xe lamp (100 W) AM1.5G filter	99.999% CO <sub>2</sub> in water bubbler at 1 atm	122.33	100	(Omr et al., 2023)	
		W <sup>6+</sup> -doped CN-W	T = ambient P = 1.013 bar V = 200 mL	Xe lamp (300 W, $\lambda$ = 320–780 nm)	0.084 g NaHCO <sub>3</sub> and H <sub>2</sub> SO <sub>4</sub> solution (2 M, 0.3 mL), producing CO <sub>2</sub> and H <sub>2</sub> O <sub>(g)</sub>	4.45	52.59	(Liang et al., 2022)	
		CsPbBr <sub>3</sub> QD/GO	V = 40 mL	Xe lamp (150 mW/cm <sup>2</sup> ) AM1.5G filter	10 mL of ethyl acetate with CO <sub>2</sub>	29.8	99.1	(Xu et al., 2017)	
		CsPbBr <sub>3</sub> -GO	V = 40 mL	Xe lamp (100 mW/cm <sup>2</sup> ) AM 1.5G and 400 nm cut-off filter	CO <sub>2</sub> gas for 30 min purged	18.6	91.5	(Chen et al., 2021)	
		Cs <sub>2</sub> AgBiBr <sub>6</sub> -Cu-RGO	T = ambient V = 125 mL	Xe lamp (100 W) AM1.5G filter	CO <sub>2</sub> gas in 125 mL reactor	10.7 (±0.6)	93 (±0.5)	(Kumar et al., 2021)	
	Photo-TMDs	TiO <sub>2</sub> /MoS <sub>2</sub>	T = 40 °C V = 200 mL	Xe arc lamp (350 W)	CO <sub>2</sub> and H <sub>2</sub> O <sub>(g)</sub> in 12 g NaHCO <sub>3</sub> and H <sub>2</sub> SO <sub>4(aq)</sub> (0.25 mL, 2 M)	2.55	-	(Xu et al., 2018)	
3D-SiC@2D-MoS <sub>2</sub>		T = 298 K P = 1.013 bar V = 40 mL	Xe lamp (300 W) ( $\lambda \geq 420$ nm filter)	Pure CO <sub>2</sub> with H <sub>2</sub> O vapor under atmospheric pressure	323 ( $\mu\text{L}\cdot\text{g}^{-1}\cdot\text{h}^{-1}$ )	~100	(Wang et al., 2018)		
MoS <sub>2</sub> /In <sub>2</sub> S <sub>3</sub>		T = 60 °C P = 0.6 MPa V = 100 mL	Xe lamp (300 W)	Pure CO <sub>2</sub> (99.99%) at 0.6 MPa	68.41	80.3	(Cai et al., 2024)		
Photo-MXene			g-C <sub>3</sub> N <sub>4</sub> /Bt/Ti <sub>3</sub> C <sub>2</sub>	P = 0.2 bar	HID lamp (20 mW/cm <sup>2</sup> , $\lambda$ = 420 nm)	CO <sub>2</sub> (99.99%) with water bubbled under reactor pressure of 0.20 bars	230	41.37	(Tahir & Tahir, 2020)
(Continued)									

(Continued)

Table 2. (Continued)

Product	Type	Materials type	Photocatalyst	Operating parameter	Light source	CO <sub>2</sub> feeding conditions	Yield ( $\mu\text{mol.g}^{-1}.\text{h}^{-1}$ )	Selectivity (%)	Ref
Photo-	LDH		LaCoO <sub>3</sub> /g-C <sub>3</sub> N <sub>4</sub> /V <sub>2</sub> C	T = ambient P = 1.013 bar V = 80 cm <sup>3</sup>	Xe lamp (20 mW/cm <sup>2</sup> , $\lambda$ = 420 nm)	CO <sub>2</sub> (99.9%) with water bubbled	332	66	(Madi & Tahir, 2024)
			meso-TiO <sub>2</sub> @ZnIn <sub>2</sub> S <sub>4</sub> / Ti <sub>3</sub> C <sub>2</sub>	None	Xe lamp (300 W, $\lambda$ = 200– 800 nm)	-	11.33	52.7	(Wang et al., 2021)
			La <sub>2</sub> Ti <sub>2</sub> O <sub>7</sub> /Ti <sub>3</sub> C <sub>2</sub>	V = 100 mL	Xe lamp (300 W)	1% CO <sub>2</sub> and 99% N <sub>2</sub> and 1 mL of H <sub>2</sub> O	11.16	12.2	(Wang et al., 2023)
			Fe <sub>3</sub> O <sub>4</sub> /Mg-Al LDH	V = 300 mL	ultraviolet light (254 nm, 8 W)	70 mL NaOH (0.1 mol/L) and 5 mL of acetonitrile under CO <sub>2</sub> gas for 30 min	223.9	-	(Gao et al., 2019)
Photo-	COFs		NiAl-LDH	T = 40 °C V = 50 mL	Xe lamp (300 W) with cutoff filter ( $\lambda$ = 600–800 nm)	CO <sub>2</sub> at pressure of 0.18 MPa	103	70.3	(Tan et al., 2019)
			EPPT-COF	V = 25 mL	Solar simulator AM1.5 G filter	CO <sub>2</sub> (99.999%) and water vapor mixture (ca. 60% relative humidity)	14.7	100	(El-Mahdy et al., 2023)
			TFPB-TRZ COF	V = 30 mL	Xe lamp (300 W) ( $\lambda$ = 420–800 nm, visible-cut filter)	CO <sub>2</sub> (99.99%) was purged into the 30 mL reactor for 30 minutes	128	~99	(Biswas et al., 2024)
Photo-	MOFs		Cu-CuTCPP/g-C <sub>3</sub> N <sub>4</sub>	T = 20 °C P = 0.1 MPa V = 100 mL	Xe lamp (150 mW/cm <sup>2</sup> ) ( $\lambda$ = 360–800 nm, UV-, IR-cut filter)	Pure CO <sub>2</sub> at 0.1 MPa	11.6	27	(Xie et al., 2022)
			TiO <sub>2</sub> @CoNi-MOF NTs	T = ambient	Xe lamp (300 W) AM1.5G filter	High-purity CO <sub>2</sub> for 30 min purged	41.65	93.2	(Liang et al., 2023)
Methanol	Metal oxides		Cu <sub>x</sub> O/TiO <sub>2</sub>	T = 60 °C P = 0.4 MPa CO <sub>2</sub>	Xe lamp (300 W)	High purity CO <sub>2</sub> at up to 0.4 MPa	53.75	98.85	(Xi et al., 2022)
			Fe-doped TiO <sub>2</sub> / SrTiO <sub>3</sub>	-	Xe lamp (100 mW/cm <sup>2</sup> ) AM1.5 filter	CO <sub>2</sub> (99.9%) with water bubble for 30 min purged	154.2	98.9	(Huang et al., 2024)
			UT-CeO <sub>x</sub>	T = ambient V = 150 mL	Xe lamp (300 W)	NaHCO <sub>3</sub> (120 mg) and 0.35 M <sub>(aq)</sub> HCl for CO <sub>2</sub> generation	1.8	97.09	(S.S et al., 2022)
			Ru/In <sub>2</sub> O <sub>3</sub>	T = 250 °C P = 1 MPa	Xe lamp (300 W)	25% CO <sub>2</sub> and 75% H <sub>2</sub> for 30 min purged	280.4	18	(Deng et al., 2023)
Photo- thermal			Bi <sub>4</sub> TaO <sub>8</sub> Cl/Bi	T = 200 °C	Xe lamp (300 W)	99.999% CO <sub>2</sub> for 20 min purged	2.34	48	(Li et al., 2022)
			g-C <sub>3</sub> N <sub>4</sub> /rGO	None	Xe lamp (300 W) AM1.5 filter	CO <sub>2</sub> degassed to remove air for 30 min	114	83	(Sahoo et al., 2022)

(Continued)

Table 2. (Continued)

Product	Type	Materials type	Photocatalyst	Operating parameter	Light source	CO <sub>2</sub> feeding conditions	Yield ( $\mu\text{mol}\cdot\text{g}^{-1}\cdot\text{h}^{-1}$ )	Selectivity (%)	Ref
Photo-thermal	TMDs	CoPc/CNT	Ag/2H-MoS <sub>2</sub>	P = 4 MPa V = 145 mL	Xe lamp (1000 W)	25% CO <sub>2</sub> and 75% H <sub>2</sub> purged	2.4 ( $\text{mmol}\cdot\text{g}^{-1}\cdot\text{h}^{-1}$ )	99	(Ren et al., 2025)
				T = 20 °C V = 75 mL	Hg lamp (250 W, $\lambda$ = 370 nm)	High-purity CO <sub>2</sub> was bubbled through isopropanol in the 75 mL reactor	365.08	-	(Zheng et al., 2019)
Photo-	MXene		MoS <sub>2</sub>	P = 0.2 MPa CO <sub>2</sub>	AM1.5G solar simulator (300 W, $\lambda$ = 320–780 nm)	CO <sub>2</sub> (99.999%) at 0.2 MPa	2.00	26	(Liu et al., 2024)
				(0.0146 $\mu\text{mol}$ of Pt)			3.41	35	
				(0.0365 $\mu\text{mol}$ of Pt)			0.58	7	
Photo-	LDH		Ti <sub>3</sub> C <sub>2</sub> /Bi <sub>2</sub> WO <sub>6</sub>	T = 4 °C V = 200 mL	Xe arc lamp (300 W, $\lambda$ > 420)	CO <sub>2</sub> gas (99.995%)	25.56	63.33	(Zhang et al., 2022)
				T = ambient P = 1.013 bar V = 200 mL	Xe lamp (300 W)	CO <sub>2</sub> generation by 0.084 g NaHCO <sub>3</sub> and 0.3 mL H <sub>2</sub> SO <sub>4</sub> (2 mol/L)	0.44	19.8	(Cao et al., 2018)
				T = 5 °C V = 500 mL	Xe lamp (300 W)	CO <sub>2</sub> at 0.06 MPa	2.07	10.4	(Wang et al., 2022)
Photo-	COFs		N <sub>3</sub> – COF A-COF	T = 80 °C P = 0.4 MPa CO <sub>2</sub> V = 132 mL	Xe lamp (500 W) ( $\lambda$ = 420–800 nm, UV- and IR-cut filter)	CO <sub>2</sub> at 0.4 MPa	13.7 8.6	- -	(Fu et al., 2018)
Photo-	MOFs		g-C <sub>3</sub> N <sub>4</sub> /CuO@MIL-125(Ti)	P = 1.0 MPa CO <sub>2</sub> V = 100 mL	Xe lamp (326.1 mW/cm <sup>2</sup> , $\lambda$ = 360–800 nm)	1.0 mL of water and 0.3% CO <sub>2</sub> until the CO <sub>2</sub> pressure reached 1.0 MPa	332.4	18.9	(Li et al., 2020)
				T = ambient	LED light ( $\lambda$ = 450 nm)	CO <sub>2</sub> for 1 h injection	44.7	100	(Batoo et al., 2024)
Ethane	Metal oxides		AgCu-TNTA	V = 32 mL	AM 1.5G Solar simulator (100 mW/cm <sup>2</sup> )	Pure CO <sub>2</sub> gas to 50 psi	14.5	60.7	(Vahidzadeh et al., 2021)
				-	LED light (50 W, $\lambda$ = 530 nm)	The CO <sub>2</sub> (3 sccm) flowing through the water bubbler, composed of ~3.1 v/v % H <sub>2</sub> O(g) and ~ 96.9 v/v% CO <sub>2</sub>	0.66	20	(Wang et al., 2021)
Photo-	Carbonaceous		Au/TiO <sub>2</sub>	T = 4 °C V = 400 mL	Xe lamp (394 mW/cm <sup>2</sup> )	80 kPa high pure CO <sub>2</sub> (99.999%)	11.07	65.88	(Ji et al., 2023)
				T = ambient	Xe lamp (415 mW/cm <sup>2</sup> )	Pure CO <sub>2</sub> gas flowing (100 mL/min)	46.1	97.5	(Jia et al., 2024)
							1.71	30.41	

(Continued)



Table 2. (Continued)

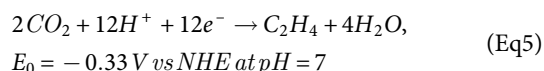
Product	Type	Materials type	Photocatalyst	Operating parameter	Light source	CO <sub>2</sub> feeding conditions	Yield ( $\mu\text{mol}\cdot\text{g}^{-1}\cdot\text{h}^{-1}$ )	Selectivity (%)	Ref
Ethylene	Photo-thermal			T = ambient P = 1.013 bar V = 200 mL	Xe lamp (300 W, $\lambda = 320\text{--}780\text{ nm}$ )	0.084 g NaHCO <sub>3</sub> and H <sub>2</sub> SO <sub>4(aq)</sub> (2 M, 0.3 mL) for producing CO <sub>2</sub> and H <sub>2</sub> O vapors			(Liang et al., 2022)
				P = 0.65 atm	Xe lamp (300 W)	CO <sub>2</sub> (99.999%) at 0.65 atm	616.6	33	(Wang et al., 2022)
				-	Xe lamp (100 mW/cm <sup>2</sup> ) AM1.5 filter	Moist CO <sub>2</sub> gas at 1 cc/min	0.0371	61.83	(Hwang et al., 2023)
				T = 30 °C V = 400 mL	Hg lamp (250 W)	CO <sub>2</sub> gas bubbled at a rate of 1.5 mL/min	6.37	47.72	(Manna et al., 2024)
	Photo-thermal	COFs	FeNi@CNTs	P = 1.013 bar	Xe lamp (300 W)	40% C <sub>2</sub> H <sub>6</sub> , 40% CO <sub>2</sub> , 20% Ar purged	768	44.7	(Zhang et al., 2023)
			MoS <sub>2</sub> @COF	T = ambient P = 1.013 bar	Xe lamp (209 mW/cm <sup>2</sup> ) ( $\lambda = 420\text{--}780\text{ nm}$ , 420 nm-cut filters)	CO <sub>2</sub> (99.999%) for 5 min purged	56.2	83.8	(Yang et al., 2023)
	Photo-thermal	MOFs	TiO <sub>2</sub> (2)@UiO-67	T = ambient	Xe lamp (300 W) ( $\lambda > 420\text{ nm}$ , cut-off filter)	CO <sub>2</sub> for 30 min purged	79.3	100	(Saadh et al., 2025)
			Cu-CuTCPP/g-C <sub>3</sub> N <sub>4</sub>	T = 20 °C P = 0.1 MPa V = 100 mL	Xe lamp (150 mW/cm <sup>2</sup> ) ( $\lambda = 360\text{--}800\text{ nm}$ , UV-and IR-cut filters)	Pure CO <sub>2</sub> purged to 0.1 MPa	18.5	44	(Xie et al., 2022)
Ethylene	Photo-thermal	Metal oxides	N-doping CeO <sub>2</sub> -AH FLPs	T = 25 °C V = 100 mL	Xe lamp (500 mW/cm <sup>2</sup> )	CO <sub>2</sub> (99.99%) for 30 minutes purged	33.18	24.91	(Van et al., 2024)
			Ni/TiO <sub>2</sub> -O <sub>v</sub>	V = 100 mL	UV-Vis (4.31 W/cm <sup>2</sup> )	1% CO <sub>2</sub> and 99% N <sub>2</sub> for 30 min purged with 1 mL water	63.8	51.2	(Si et al., 2025)
			Cu <sub>x</sub> P/g-C <sub>3</sub> N <sub>4</sub>	P = 85.0 kPa V = 250 mL	Xe lamp (150 mW/cm <sup>2</sup> , $\lambda = 320\text{--}780\text{ nm}$ )	CO <sub>2</sub> (99.999%) to 85.0 kPa	3.58	64.25	(Wen et al., 2025)
	Photo-thermal	TMDs	MoS <sub>2</sub> /Fe <sub>2</sub> O <sub>3</sub>	V = 50 mL	Xe lamp (100 mW/cm <sup>2</sup> )	CO <sub>2</sub> degassed to remove air	10.6	48.4	(Song et al., 2024)
			WO <sub>2.9</sub> /WTe <sub>2</sub>	-	Xe lamp (300 W)	high-purity CO <sub>2</sub> to ambient pressure	122.9	78	(Zhang et al., 2024)
	Photo-thermal	MOFs	R-MOF-74(Cu)	T = 25 °C P = 80 kPa	Xe lamp (300 W)	50 mL H <sub>2</sub> O and CO <sub>2</sub> at 80 kPa	1.3	90.2	(Wang et al., 2025)
			Zr/Cu <sub>29</sub> -UiO-67	T = 25 °C	Xe lamp (300 W, $\lambda > 420\text{ nm}$ )	CO <sub>2</sub> for 15 min purged	69.1	100	(Asiri et al., 2025)

(Continued)

Table 2. (Continued)

Product	Type	Materials type	Photocatalyst	Operating parameter	Light source	CO <sub>2</sub> feeding conditions	Yield ( $\mu\text{mol}\cdot\text{g}^{-1}\cdot\text{h}^{-1}$ )	Selectivity (%)	Ref
Photo-	TMDs		$\text{Bi}_2\text{S}_3/\text{In}_2\text{S}_3$	T = 25 °C P = 1.013 bar V = 170 mL	Xe lamp (0.2 W/cm <sup>2</sup> , $\lambda = 320\text{--}780\text{ nm}$ )	Pure CO <sub>2</sub> with 1 mL DI water	11.81	90	(Yan et al., 2023)
			$\text{W}_{18}\text{O}_{49}/\text{WTe}_2$	P = 1.013 bar	Xe lamp (300 W)	high-purity CO <sub>2</sub> to ambient pressure with 0.4 mL DI water	147.6 ( $\mu\text{mol}\cdot\text{g}^{-1}$ )	80	(Zhang et al., 2024)
			WTe <sub>2</sub>	T = 185 °C P = 1.013 bar	Xe lamp (300 W)	high-purity CO <sub>2</sub> to ambient pressure with 0.4 mL DI water	115.51 ( $\mu\text{mol}\cdot\text{g}^{-1}$ )	88	(Zhang et al., 2024)

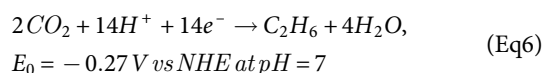
as C<sub>1</sub> products. The representative 12-electron reduction for ethylene is as follows:



To improve C<sub>2</sub> product selectivity, strategies such as heterojunction engineering, defect modification, light-harvesting enhancement, and surface activation have been explored. For instance, Xu *et al.* designed a nitrogen-doped CeO<sub>2</sub> photocatalyst featuring surface-frustrated Lewis pairs (FLPs) of Ce<sup>3+</sup>/Ce-OH, enhancing CO<sub>2</sub> activation and C-C coupling. This catalyst produced CO (224.56 μmol·g<sup>-1</sup>·h<sup>-1</sup>, 28.1%), C<sub>2</sub>H<sub>4</sub> (33.18 μmol·g<sup>-1</sup>·h<sup>-1</sup>, 24.91%), and C<sub>2</sub>H<sub>2</sub> (25.84 μmol·g<sup>-1</sup>·h<sup>-1</sup>, 16.16%) (Yan *et al.*, 2024). MOFs also offer promise. A Zr/Cu bimetallic UiO-67 MOF improved electron transfer and C-C coupling efficiency, achieving selective C<sub>2</sub>H<sub>4</sub> production (69.1 μmol·g<sup>-1</sup>·h<sup>-1</sup>, 100% selectivity) (Asiri *et al.*, 2025). Moreover, non-stoichiometric WO<sub>3-x</sub> (particularly WO<sub>2.9</sub>) exhibits enhanced visible/NIR absorption and reactivity due to oxygen vacancies (Lu *et al.*, 2020). Tu *et al.* synthesized a WO<sub>2.9</sub>/WTe<sub>2</sub> photothermal catalyst that demonstrated a high ethylene production rate of 122.9 μmol·g<sup>-1</sup> and a selectivity of 78%. When the reaction temperature was elevated to 240 °C, the ethylene yields significantly increased to 475.3 μmol·g<sup>-1</sup>. The WO<sub>2.9</sub> component plays a key role in bandgap modulation and CO<sub>2</sub> adsorption through its abundant oxygen vacancies, while WTe<sub>2</sub> effectively stabilizes aldehyde intermediates, enriching the catalyst surface with reactive species and facilitating efficient C-C bond formation (Zhang *et al.*, 2024).

### Production of ethane

The photocatalytic reduction of CO<sub>2</sub> to ethane (C<sub>2</sub>H<sub>6</sub>) involves a 14-electron transfer process and the formation of multiple reactive intermediates. The overall reduction reaction is represented as:



Mechanistically, the surface-mediated C-C coupling of methyl (\*CH<sub>3</sub>) radicals, which is necessary for the generation of C<sub>2</sub><sup>+</sup> hydrocarbons, poses challenges to the progression of the reaction. To overcome these limitations, researchers have fabricated dual-atom catalysts, exemplified by incorporating phosphorus and copper single-atom sites on carbon nitride nanosheets (P/CuSAs@CN). This photocatalyst achieved an ethane production rate of 616.6 μmol·g<sup>-1</sup>·h<sup>-1</sup> with a selectivity of 33%. The Cu and P atoms serve as electron and hole trapping sites within the carbon nitride matrix, facilitating charge separation and accumulation at Cu sites, which is vital for driving multi-electron transfer steps. *In situ* FTIR spectroscopy identified key intermediates, including \*CO and \*OCCOH, confirming the involvement of hydrogenation of \*OCCO as the rate-determining step in C<sub>2</sub>H<sub>6</sub> formation (Wang *et al.*, 2022). The COFs and MOFs offer strong potential in photocatalysis due to their π-conjugated structures, which support charge transport and light absorption (Saadh *et al.*, 2025). Bai *et al.* developed a MoS<sub>2</sub>@COF hybrid by covalently integrating amino-modified MoS<sub>2</sub> with an anthraquinone-based COF, achieving an ethane production rate of 56.2 μmol·g<sup>-1</sup>·h<sup>-1</sup> and 83.8% selectivity under visible light, significantly outperforming individual components. *In situ* DRIFTS and DFT analyses confirmed that the hybrid promotes CO<sub>2</sub> adsorption, CO hydrogenation, and C-C coupling, facilitating efficient C<sub>2</sub>H<sub>6</sub> formation (Yang *et al.*, 2023).

## Photothermal catalytic reaction systems

Photothermal CO<sub>2</sub> conversion leverages solar or near-infrared irradiation to generate localized heating and, in some cases, hot electrons, thereby enhancing CO<sub>2</sub> hydrogenation efficiency (Guo *et al.*, 2023; Gao *et al.*, 2020; Cai *et al.*, 2021). Effective photothermal catalysts must exhibit synergistic properties, including strong light absorption and efficient thermal confinement (e.g., incorporation of core-shell structures, plasmonic coupling, or defect engineering) (Cai *et al.*, 2021; Feng *et al.*, 2020; Tang *et al.*, 2025; Li *et al.*, 2024). To date, significant progress has been made in producing light hydrocarbons, particularly methane, through photothermal conversion. Additionally, several studies have explored photothermal catalytic reactions to synthesize carbonates, such as dimethyl carbonate (DMC) and glycerol carbonate (GC), which have been scarcely reported in photocatalytic systems. Relevant findings are summarized in the following sections.

### The production of C<sub>1</sub> and C<sub>2</sub> chemicals

Similar to photocatalytic conversion, the production of C<sub>1</sub> and C<sub>2</sub> chemicals via photothermal catalytic reduction of CO<sub>2</sub>, involving the use of gaseous hydrogen (*i.e.*, photothermal hydrogenation) and/or water, has attracted attention. The experimental conditions, as well as the key performance indicators of these systems, are summarized in Table 2 for comparison with those from photocatalytic reduction systems. Among these pathways, the development in photothermal methanation systems has the most progress. Catalyst such as MXene-supported metal (e.g., Ni/Nb<sub>2</sub>C [Wu *et al.*, 2021]), metal nanoparticles (e.g., plasmonic Co-SiO<sub>2</sub> superstructures [Cai *et al.*, 2024], Ru/MnCo<sub>2</sub>O<sub>4</sub> [Guo *et al.*, 2023]), single-atom catalysts (e.g., the Ru-F<sub>4</sub> configuration [Tang *et al.*, 2024]), and core-shell designs (e.g., Ni@p-SiO<sub>2</sub> [Cai *et al.*, 2021]) have been reported successful for photothermal CO<sub>2</sub> conversion to light hydrocarbons.

As illustrated in Table 2, photothermal catalytic reduction systems generally achieve higher product yield or selectivity than photocatalytic reduction processes, especially when hydrogen or water is used as co-reactants. For example, photothermal methanation systems exhibit greater reaction efficiency, with product yields reaching mmol·g<sup>-1</sup>·h<sup>-1</sup> (or mol·g<sup>-1</sup>·h<sup>-1</sup>) levels (Guo *et al.*, 2023; Guo *et al.*, 2025), compared to photocatalytic reactions that typically yield μmol·g<sup>-1</sup>·h<sup>-1</sup>. Several studies also demonstrate successful photothermal methanation in flow systems (Guo *et al.*, 2023; Wu *et al.*, 2021; Tang *et al.*, 2024), indicating potential for scale-up. Moreover, unlike most photocatalytic systems driven by lamp irradiation, successful photothermal systems for CO<sub>2</sub>-based light olefin (Ning *et al.*, 2024) and syngas (Wu *et al.*, 2025) have been demonstrated using full sunlight, underscoring their potential.

Nonetheless, these systems often require higher temperatures and pressures, reducing the inherent benefits of photocatalytic methods. Moreover, the dependence on hydrogen poses a major challenge, particularly in areas without access to green hydrogen or the infrastructure for sustainable hydrogen production. Therefore, it is crucial to evaluate whether these improvements justify practical implementation.

### Production of dimethyl carbonate (DMC)

The formation of DMC requires the reaction of CO<sub>2</sub> with methanol. Prior research has reported the successful use of CeO<sub>2</sub>-based catalysts enriched with oxygen vacancies, which have proven to be efficient for this purpose.

Within the limited volume of previous studies, Guan *et al.* synthesized Bi<sup>3+</sup>-doped Ce<sub>x</sub>Bi<sub>1-x</sub>O<sub>2-δ</sub> nanorods (Guan *et al.*,

2024), achieving a DMC yield of  $3.13 \text{ mmol}\cdot\text{g}^{-1}$  at  $140^\circ\text{C}$  and  $1.6 \text{ MPa}$  under photo-irradiation, attributing performance gains to asymmetric Bi-O-Ce oxygen vacancies that improve  $\text{CO}_2$  activation and light absorption efficiency. Bai *et al.* employed a low-temperature plasma-driven technique to introduce corner defects into quadrangular pyramid-octahedral  $\text{CeO}_2$  (Bai *et al.*, 2023). This approach achieved a DMC yield of 1.58%, corresponding to an eightfold increase relative to conventional thermal catalysis performed at  $140^\circ\text{C}$  and  $7.5 \text{ MPa}$ . Jin *et al.* prepared  $\text{CeO}_2$  nanorods with bifunctional oxygen vacancies via a template-free hydrothermal method (Jin *et al.*, 2023). This method resulted in improved photothermal catalytic activity, evidenced by a DMC yield of  $17.7 \text{ mmol}\cdot\text{g}^{-1}\cdot\text{h}^{-1}$  under relatively mild reaction conditions ( $140^\circ\text{C}$ ,  $1.6 \text{ MPa}$ ). The enhanced performance was attributed to increased  $\text{CO}_2$  adsorption capacity and the inhibition of recombination of photo-induced electron-hole pairs.

### Production of glycerol carbonate (GC)

The direct conversion of  $\text{CO}_2$  and glycerol to glycerol carbonate (GC) offers a promising solution to two environmental wastes. Within the currently limited findings, Liu *et al.* developed  $\text{Au}/\text{ZnWO}_4\text{-ZnO}$  catalysts for photothermal conversion of glycerol and  $\text{CO}_2$  into GC, where Au nanoparticles enhanced performance via localized surface plasmon resonance (LSPR) under visible light and heat, significantly boosting GC yield compared to thermal catalysis (Liu *et al.*, 2019). Liu *et al.* also reported a  $\text{Co}_3\text{O}_4\text{-ZnO}$  p-n heterojunction catalyst, achieving a GC yield of 5.3% at  $150^\circ\text{C}$  and  $5 \text{ MPa}$   $\text{CO}_2$  under visible light (Liu *et al.*, 2022). The p-n heterojunction effectively increased visible light absorption and electron-hole separation, breaking the thermodynamic limitations of conventional thermal catalysis. Li *et al.* further improved the  $\text{Co}_3\text{O}_4\text{-ZnO}$  system by decorating it with Au nanoparticles to create  $\text{Au}/\text{Co}_3\text{O}_4\text{-ZnO}$  catalysts (Li *et al.*, 2024). This strategy generated surface oxygen vacancies, enhanced visible-light absorption, and increased GC yield to 6.5% under the same photothermal conditions ( $150^\circ\text{C}$ ,  $5 \text{ MPa}$   $\text{CO}_2$ ) due to improved electron-hole separation. Additionally, Li *et al.* explored  $\text{La}_2\text{O}_2\text{CO}_3\text{-ZnO}$  catalysts (Li *et al.*, 2021), demonstrating strong photothermal synergy in glycerol carbonylation, achieving a 6.9% glycerol conversion under irradiation at  $150^\circ\text{C}$  and  $5.5 \text{ MPa}$   $\text{CO}_2$ . The synergistic interaction between  $\text{La}_2\text{O}_2\text{CO}_3$  and ZnO played a crucial role in this enhanced catalytic performance.

### Standard procedure of photocatalytic $\text{CO}_2$ conversion

The standard method for photocatalytic  $\text{CO}_2$  conversion involves light sources (e.g., calibrated lamps or solar simulators), photoreactors, gas delivery systems, photocatalysts, and analytical tools for product analysis. Photoreactors are typically configured as suspended systems, where the catalyst is dispersed in a liquid (slurry reactors), or as heterogeneous systems, such as fixed-bed or monolithic reactors. Quartz or other optical-grade windows are essential for optimal light transmission. Selecting functionalized photocatalysts (detailed in Section “Fundamentals of photocatalytic conversion”) enhances charge separation and light absorption during  $\text{CO}_2$  conversion (Kou *et al.*, 2017). Before starting the reaction, the reactor is leak-tested, purged with high-purity  $\text{CO}_2$  or inert gas, and equilibrated to the desired temperature and pressure.

In suspended catalytic systems, reactions mainly occur in the liquid phase, where  $\text{CO}_2$  dissolves in an alkaline solution to promote the reaction. This process produces both gaseous products (e.g., methane, carbon monoxide) and liquid products (e.g., methanol), with liquid products often dominating due to fewer electron

transfers. Conversely, heterogeneous systems enable gas-phase reactions that primarily yield methane. Gaseous hydrogen is continuously fed into the reactor to react with  $\text{CO}_2$ , resembling conventional hydrogenation reactors. These features can be combined to create biphasic photocatalytic conversion systems (Bonchio *et al.*, 2023; Variar *et al.*, 2021).

Controlled irradiation is applied using a calibrated AM 1.5G solar simulator or equivalent light source, with precise regulation of temperature and  $\text{CO}_2$  pressure to influence product selectivity. For example, lower temperatures ( $\sim 70^\circ\text{C}$ ) favor CO formation, whereas higher temperatures ( $100\text{--}120^\circ\text{C}$ ) promote methane production. Regarding pressure effects, moderate  $\text{CO}_2$  pressures ( $\sim 110 \text{ kPa}$ ) optimize methanol synthesis, whereas higher pressures ( $>130 \text{ kPa}$ ) enhance methane generation (Meesattham & Kim-Lohsoontorn, 2022; Yang *et al.*, 2022). Throughout the reaction, gaseous and liquid products are periodically sampled and quantified using gas chromatography, liquid chromatography, or nuclear magnetic resonance spectroscopy, employing appropriate calibration standards. Overall, thorough documentation of catalyst properties, reactor setup, operational parameters, and error analysis is essential for scientific rigor and study comparability.

### Modeling

Currently, advancements in the modeling of photocatalytic and photothermal catalytic processes remain constrained (Jesic *et al.*, 2021; Kovacic *et al.*, 2020). Existing studies have primarily focused on the macroscopic description of photoreactors, including slurry reactors (Asadi *et al.*, 2022), fixed-bed reactors (Rastgaran *et al.*, 2023), twin reactors (Lu *et al.*, 2021), and others (Ramayashree *et al.*, 2024). The most comprehensive studies employed mathematical modeling (Ray, 1999) or even computational fluid dynamics (CFD) (Lu *et al.*, 2021) to conduct multiphysics simulations, attempting to characterize the flow field, velocity distribution, reactor geometry, and mass transfer within the reactor.

To our knowledge, there is a notable lack of process concepts for photocatalytic  $\text{CO}_2$  conversion in the literature, primarily due to several challenges. First, kinetic modeling is particularly difficult because it requires understanding interfacial behavior, various interactions (e.g., adsorption, desorption), site balance, and the effects of irradiation. Quantum approaches may help clarify these factors (Jesic *et al.*, 2021; Kovacic *et al.*, 2020). Secondly, most experiments use diluted reaction media, resulting in low product yield and selectivity, complicating separation processes. Furthermore, reactor performance depends on its dimensions and irradiation conditions. Consequently, most models have focused on specific experimental setups, limiting the predictive capability.

### From experimentation to processes

Despite extensive experimental research, photocatalytic  $\text{CO}_2$  conversion technologies have not yet reached their full potential. Key challenges include low yield, limited selectivity, and inefficient light utilization. This section proposes process configurations tailored to various photocatalytic conversion types, combining current experimental results with practical process insights.

### Process consideration of the photocatalytic reduction of $\text{CO}_2$

From a macroscopic perspective, several experimental challenges must be addressed before scaling up photocatalytic  $\text{CO}_2$  reduction. First, most photocatalytic  $\text{CO}_2$  reduction reactions occur in the

liquid phase within suspended catalytic systems, producing hydrocarbons and methanol as the main products, with water as the hydrogen source. Due to the low solubility of CO<sub>2</sub> in the aqueous phase (approximately 0.033 mol per liter at 25 °C and 1 atm), reactions are typically conducted in alkaline solutions. This complicates downstream separation and recovery of photocatalysts and alkaline agents.

Figure 1a depicts a process configuration for hydrocarbon synthesis via photoreduction, which is proposed based on current knowledge. The process begins with capturing CO<sub>2</sub> from point emission sources (e.g., flue gas) through chemical absorption, using the alkaline solvent. After absorption, the rich solvent undergoes photocatalytic reduction in a photoreactor. Note that this rich solvent has a composition similar to that in typical photocatalytic conditions. Hydrocarbon products, being only slightly soluble, can be separated easily by vapor–liquid separation. The next step should isolate hydrocarbons from CO<sub>2</sub> using physical methods, such as adsorption and membrane techniques. If hydrocarbon concentration is low, it is more practical to use the effluent as gas fuel rather than purifying it for marketable products. Downstream of the photoreactor, alkaline solution recovery can be achieved through regeneration methods such as causticization (with CO<sub>2</sub> stripping) and electrodialysis (Mahmoudkhani & Keith, 2009; Sabatino et al., 2022).

In addition, photocatalytic reaction can also be integrated with the direct air capture (DAC) process. Currently, the main challenge in DAC is the very low concentration of CO<sub>2</sub> in the atmosphere (approximately 400 ppm). However, using a strong alkaline solution as an absorbent can selectively capture CO<sub>2</sub> from nitrogen and oxygen while simultaneously providing suitable conditions for the photocatalytic reduction of CO<sub>2</sub>. This synergistic effect may offer additional benefits for the future application of DAC.

To improve system performance, advanced photocatalysts that rapidly convert CO<sub>2</sub> under vapor–liquid equilibrium are essential. Fast kinetics enable continuous CO<sub>2</sub> dissolution in the alkaline solution, promoting ongoing reduction. Reducing mass transfer resistance is also crucial. Conversely, increasing system pressure offers only marginal gains in CO<sub>2</sub> solubility and undermines the benefit of milder operating conditions in photocatalytic conversion.

Figure 1b illustrates a proposed process configuration for the synthesis of methanol (or other oxygenates) via photoreduction. A similar process layout is observed in the integration of CO<sub>2</sub> capture with the photoreactor. Since the main products are in the liquid phase, downstream separation is challenging due to the low experimental yield (<1 wt%). Multiple distillation columns will likely be needed for purification. If the oxygenates have higher boiling points than water, distillation becomes more difficult, as large volumes of water must be removed. Additionally, alkaline regeneration is required. These factors cause high energy consumption, leading to economic and environmental impacts.

Process intensification strategies offer opportunities to improve the performance of such processes. For example, membrane-assisted distillation (Li et al., 2019), which removes the bulk volume of water prior to distillation, may be a viable option. Furthermore, the gas effluent, which comprises CO, CH<sub>4</sub>, or H<sub>2</sub>, can subsequently be redirected to other facilities for the synthesis of additional chemical compounds (Liu et al., 2022; Wang et al., 2023).

To enable continuous operation of this process using solar energy, the reactor can be irradiated and activated by sunlight during the day, while power lamps provide illumination at night. To support this approach, additional facilities can be developed to capture and store excess solar energy during the day, which can then be used to supply power at night.

### Photothermal catalytic conversion to form carbonates

The photothermal conversion of CO<sub>2</sub> and glycerol to GC shows promising results, with the highest yields reaching approximately 6%. This yield significantly surpasses the equilibrium conversion of the direct reaction of CO<sub>2</sub> and glycerol. Therefore, this pathway is more relevant to industrial applications, and process design can be considered.

Figure 1c illustrates a potential process configuration for producing GC through the photothermal catalytic conversion of CO<sub>2</sub> and glycerol. This process flow diagram is based on the experiment conducted by Li et al. (2021), who performed the photothermal catalytic reaction in the presence of dimethylformamide (DMF). In this process, CO<sub>2</sub> from the gas source is captured by an aqueous amine solvent, and DMF is used as a co-solvent to provide a synergistic effect for CO<sub>2</sub> capture. After the reaction, the effluent contains amine, DMF, GC, and unreacted glycerol, which can be separated through a distillation sequence. Since both DMF and amine enter the absorber, further separation of these species is unnecessary. Additionally, the recovered glycerol can be recycled back to the reactor inlet. Moreover, an amine reclaiming section is required to recover and remove the degraded portion generated during the capture process. Similar to Figure 1b, the gaseous effluent can be used either for downstream chemical production or solely as a fuel gas.

In contrast, previous studies have demonstrated that the yields of DMC obtained via photothermal conversion can exceed those achieved through direct thermal conversion methods, while operating at lower pressures (photothermal: 15 to 25 bar; thermal: 30 to 50 bar). However, the overall conversion has consistently remained below 0.5%, resulting in a significantly low concentration of DMC after the reaction. Moreover, the formation of an azeotrope between DMC and methanol introduces additional complexities to the purification process. Consequently, we consider the current status of this process to be far from suitable for industrial application.

### Economic and environmental prospects on photocatalytic CO<sub>2</sub> conversion

Due to uncertainties in process development, it remains unclear whether the photocatalytic process can be economically or environmentally favorable compared to existing technologies. Currently, there is a lack of standardized metrics to evaluate the photocatalytic processes, whether from experimental data (e.g., quantum yield, turnover frequency, solar-to-fuel conversion efficiency) or process modeling (e.g., techno-economic and environmental indicators). However, previous assessments based on thermal catalytic processes may provide a foundational reference for evaluating photocatalytic processes.

Figure 2 presents a comparative analysis of the economic feasibility and decarbonization potential of different thermal catalytic CO<sub>2</sub> conversion processes, drawing upon data from our prior studies (Uddin et al., 2022; Chiu & Yu, 2024a,b; Chiou et al., 2023; Yu et al., 2018; Wu et al., 2024). The x-axis shows the ratio of the minimum selling price (MSP, set to achieve a 15% internal rate of return) to the current market price. The y-axis represents the ratio of net decarbonization potential from the process design scenario to the theoretical CO<sub>2</sub> uptake. Conceptually, processes in the upper-left quadrant indicate simultaneous economic and decarbonization benefits. However, a trade-off between economics and decarbonization potential can be identified from Figure 2. Specifically, the use of green hydrogen in hydrogenation processes offers greater



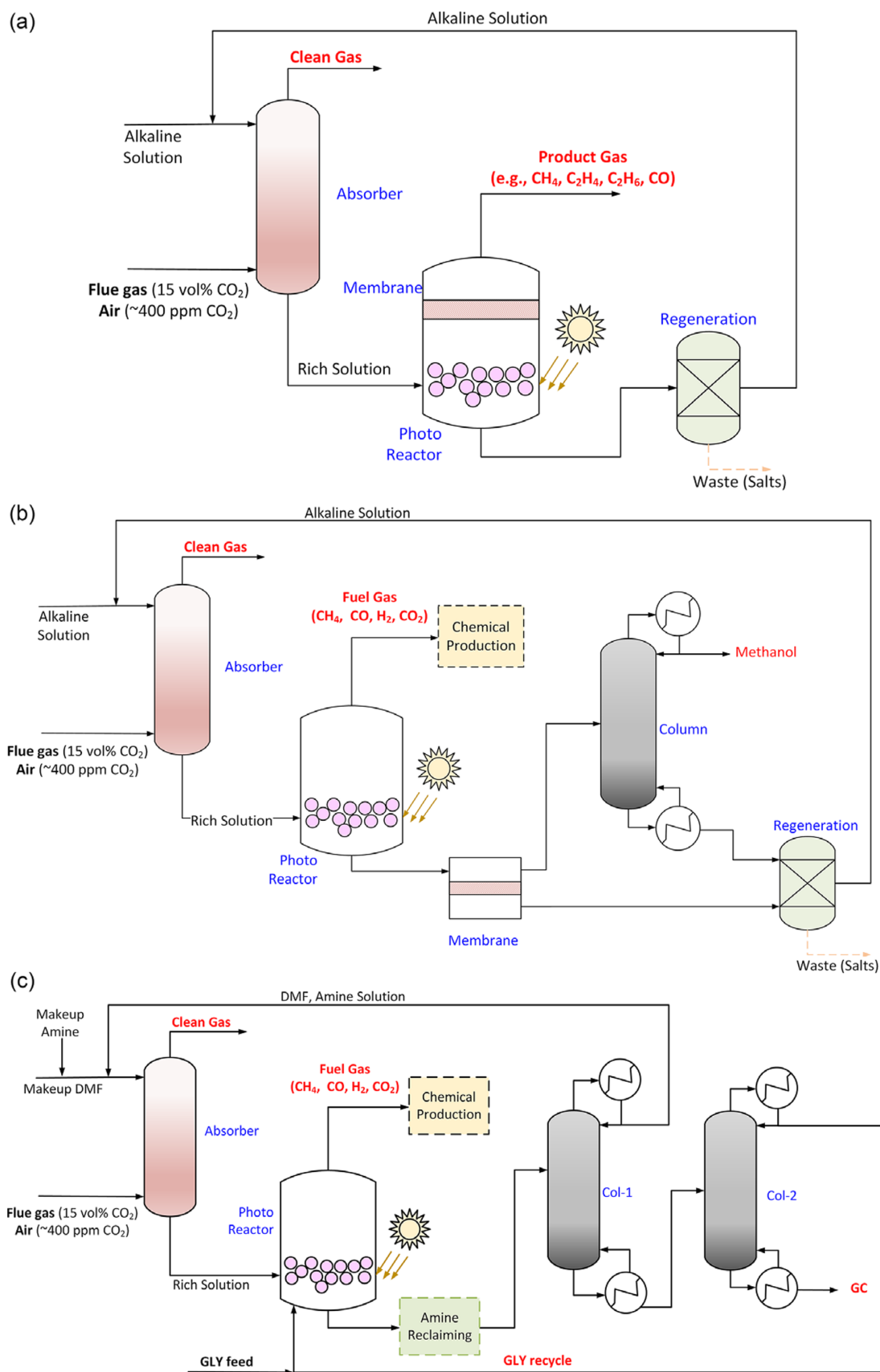


**Figure 1.** Proposed conceptual configuration of the photocatalytic conversion processes. (a) Production of hydrocarbons; (b) Production of methanol (or oxygenates); (c) Production of GC.



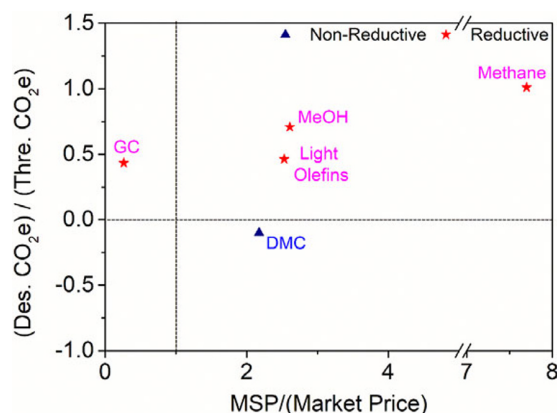


**Figure 2.** Comparison of economic and decarbonization performances across the previously studied thermal-based CO<sub>2</sub> conversion process.

decarbonization potential, while its currently high cost limits its economic feasibility (Uddin et al., 2022; Chiu & Yu, 2024a,b; Chiou et al., 2023). In contrast, producing value-added chemicals offers a better economic outlook but has limited decarbonization potential, due to low theoretical CO<sub>2</sub> uptake and high energy requirements for process purification. (Yu et al., 2018). Among various investigations, solely the GC process—which entails the indirect conversion of CO<sub>2</sub> and glycerol using propylene oxide as a co-reactant—demonstrates the potential to simultaneously attain economic viability and decarbonization.

In terms of economic and environmental aspects, the photocatalytic conversion process offers several advantages. Notably, photocatalytic CO<sub>2</sub> reduction may eliminate the need for green hydrogen, which is economically advantageous for countries struggling to produce hydrogen in a global net-zero economy. Furthermore, its ability to operate with minimal or no thermal electricity consumption could further reduce indirect greenhouse gas emissions. However, the practical deployment of photocatalytic processes is hindered by low product yields, which pose challenges and lead to economic and environmental impacts during separation. The incorporation of a solution phase, either as an alkali solution or by adding a solvent, adds complexity to the separation process. Although improving productivity is often emphasized in the literature, a quantitative framework to assess when yield (or conversion) becomes economically and environmentally viable is still lacking.

To address the aforementioned issues, it is highly recommended to implement process design and conduct a comprehensive evaluation that considers both the reaction and separation sections. Recently, Huang and Yu proposed a framework that compares the potential of the photothermal catalytic GC production process in terms of economics, environmental impact, and safety (Huang & Yu, 2025). Their study quantified that the product yield of the photothermal process must be doubled from its current highest value (6.9%) to achieve performance metrics comparable to those of existing processes. The modeling framework developed in their work provides a foundational basis for future investigations of other photocatalytic systems.

## Conclusion

This paper presents a comprehensive review of recent advancements in photocatalytic and photothermal catalytic CO<sub>2</sub> conversion processes. Experimental results related to the synthesis of

methane, methanol, C<sub>2</sub> hydrocarbons, dimethyl carbonate, and glycerol are summarized. Additionally, potential process configurations for the production of these chemicals are conceptually proposed. Currently, enhancing the product yield of photocatalytic CO<sub>2</sub> conversion is of paramount importance. Experimental research indicates that the development of novel catalysts, which are characterized by faster reaction kinetics, improved stability, and extended excited-state lifetimes, is essential. Additionally, optimizing the reaction system by minimizing mass transfer limitations can significantly improve operational efficiency. From a process development perspective, integrating concepts that combine CO<sub>2</sub> capture, photoreactor design, and downstream separation is crucial. Technological feasibility should be evaluated through comprehensive techno-economic analyses, life cycle assessments, and safety evaluations. Overall, photocatalytic CO<sub>2</sub> conversion presents inherent advantages for achieving a net-zero economy. However, substantial further research is necessary to realize its full potential.

**Open peer review.** To view the open peer review materials for this article, please visit <http://doi.org/10.1017/cat.2025.10008>.

**Author contribution.** **Ting-En Su:** Data curation, Investigation, Methodology, Writing (original draft). **Yu-Xuan Chen:** Data curation, Investigation, Methodology, Writing (original draft). **Ting-Wei Huang:** Data curation, Investigation, Methodology, Writing (original draft). **Yi-Hsin Chien:** Conceptualization, Writing (original draft), Writing (review and editing), Supervision, Project administration, Funding acquisition. **Bor-Yih Yu:** Conceptualization, Writing (original draft), Writing (review and editing), Supervision, Project administration, Funding acquisition.

**Financial support.** The research funding from the National Science and Technology Council of R.O.C. (grant number: 113–2218-E-002-027) is greatly appreciated. Y. -H. Chien appreciates the financial support provided by the National Science and Technology Council (NSTC 113–2113-M-035-001).

**Competing interests.** The authors declare that they have no known competing financial interests or personal relationships that could have appeared to influence the work reported in this paper.

## References

- Ahlers SJ, Bentrup U, Linke D and Kondratenko EV (2014) An innovative approach for highly selective direct conversion of CO<sub>2</sub> into propanol using C<sub>2</sub>H<sub>4</sub> and H<sub>2</sub>. *ChemSusChem* 7(9), 2631–2639.
- Ahmad MI, Liu Y, Wang Y, Cao P, Yu H, Li H, Chen S and Quan X (2025) Enhanced photocatalytic synthesis of urea from co-reduction of N<sub>2</sub> and CO<sub>2</sub> on Z-schematic SrTiO<sub>3</sub>-FeS-CoWO<sub>4</sub> Heterostructure. *Angewandte Chemie International Edition* 64(7), e202419628.
- Alassmy YA, Paalman PJ and Pescarmona PP (2021) One-pot fixation of CO<sub>2</sub> into glycerol carbonate using ion-exchanged Amberlite resin beads as efficient metal-free heterogeneous catalysts. *ChemCatChem* 13(1), 475–486.
- Altintas C, Erucar I and Keskin S (2022) MOF/COF hybrids as next generation materials for energy and biomedical applications. *CrystEngComm* 24(42), 7360–7371.
- Asadi A, Larimi A, Jiang Z and Naderifar A (2022) Modeling and simulation of photocatalytic CO<sub>2</sub> reduction into methanol in a bubble slurry photoreactor. *Chemical Engineering Science*, 263.
- Asiri M, Altalbawy FMA, Sead FF, Makasana J, M M, Pathak R, Juneja PK, Kumar B and Saydaxmetova A (2025) Hetero bimetallic Zr–O–Cu in UiO-67 MOF for selective and efficient CO<sub>2</sub> photoreduction to ethylene. *Journal of Molecular Structure* 1328, 141306.
- Bai JQ, Lv LL, Liu JY, Wang Q, Cheng Q, Cai MD and Sun S (2023) Control of CeO<sub>2</sub> defect sites for photo- and thermal- synergistic catalysis of CO<sub>2</sub> and methanol to DMC. *Catalysis Letters* 153(11), 3209–3218.
- Batoo KM, Ali E, Hussein SA, Chandra S, Abdulwahid AS, Kareem SH, Ijaz ME, Omran AA, Abid MK and Alawadi A (2024) UiO-67 metal-organic

- frameworks with dual amino/iodo functionalization, and mixed Zr/Ce clusters: Highly selective and efficient photocatalyst for CO<sub>2</sub> transformation to methanol. *Journal of Molecular Structure* **1312**, 138492.
- Biswas S, Rahimi FA, Saravanan RK, Dey A, Chauhan J, Surendran D, Nath S and Maji TK (2024) A triazole-based covalent organic framework as a photocatalyst toward visible-light-driven CO<sub>2</sub> reduction to CH<sub>4</sub>. *Chemical Science* **15**(39), 16259–16270.
- Bonchio M, Bonin J, Ishitani O, Lu TB, Morikawa T, Morris AJ, Reisner E, Sarkar D, Toma FM and Robert M (2023) Best practices for experiments and reporting in photocatalytic CO<sub>2</sub> reduction. *Nature Catalysis* **6**(8), 657–665.
- Cai MJ, Li CR, An XD, Zhong BQ, Zhou YX, Feng K, Wang SH, Zhang CC, Xiao MQ, Wu ZY, He JR, Wu CP, Shen JH, Zhu ZJ, Feng K, Zhong J and He L (2024) Supra-Photothermal CO<sub>2</sub> Methanation over greenhouse-like Plasmonic superstructures of Ultrasmall cobalt nanoparticles. *Advanced Materials* **36**(9).
- Cai W, Qian Z, Hu C, Zheng W, Luo L and Zhao Y (2024) Systematic investigation of MoS<sub>2</sub>-metal sulfides (metal = In, Sn, Cu, Cd) heterostructure via metal-sulfur bond for photocatalytic CO<sub>2</sub> reduction. *Chemical Engineering Journal* **479**, 147718.
- Cai MJ, Wu ZY, Li Z, Wang L, Sun W, Tountas AA, Li CR, Wang SH, Feng K, Xu AB, Tang SL, Tavasoli A, Peng MW, Liu WX, Helmy AS, He L, Ozin GA and Zhang XH (2021) Greenhouse-inspired supra-photothermal CO<sub>2</sub> catalysis. *Nature Energy* **6**(8), 807–814.
- Cao GQ, Handler RM, Luyben WL, Xiao Y, Chen CH and Baltrusaitis J (2022) CO<sub>2</sub> conversion to syngas via electrification of endothermal reactors: Process design and environmental impact analysis. *Energy Conversion and Management* **265**, 115763.
- Cao S, Shen B, Tong T, Fu J and Yu J (2018) 2D/2D heterojunction of ultrathin MXene/Bi<sub>2</sub>WO<sub>6</sub> Nanosheets for improved photocatalytic CO<sub>2</sub> reduction. *Advanced Functional Materials* **28**(21), 1800136.
- Chaban VV, Andreeva NA, Santos LM and Einloft S (2024) Sodium chloride catalyzes valorization of carbon dioxide into dimethyl carbonate. *Journal of Molecular Liquids*, **394**, 123743.
- Chen J, Lu J, Lang R, Wang C, Bao S, Li Y, Li K and Fan M (2025) Enhanced and selective photocatalytic reduction of CO<sub>2</sub> to CH<sub>4</sub> using a Pt-loaded CuPc/g-C<sub>3</sub>N<sub>4</sub> Z-scheme heterojunction catalyst. *Green Energy & Environment* **10** (6), 1348–1458.
- Chen Y-H, Ye J-K, Chang Y-J, Liu T-W, Chuang Y-H, Liu W-R, Liu S-H and Pu Y-C (2021) Mechanisms behind photocatalytic CO<sub>2</sub> reduction by CsPbBr<sub>3</sub> perovskite-graphene-based nanoheterostructures. *Applied Catalysis B: Environmental* **284**, 119751.
- Chiou HH, Lee CJ, Wen BS, Lin JX, Chen CL and Yu BY (2023) Evaluation of alternative processes of methanol production from CO<sub>2</sub>: Design, optimization, control, techno-economic, and environmental analysis. *Fuel* **343**, 127856.
- Chiu HH and Yu BY (2024a) Synthesis of green light olefins from direct hydrogenation of CO<sub>2</sub>. Part I: Techno-economic, decarbonization, and sustainability analyses based on rigorous simulation. *Journal of the Taiwan Institute of Chemical Engineers* **156**, 105340.
- Chiu HH and Yu BY (2024b) Synthesis of green light olefins from direct hydrogenation of CO<sub>2</sub>. Part II: Detailed process design and optimization. *Journal of the Taiwan Institute of Chemical Engineers* **155**, 105287.
- Chu MN, Li Y, Cui K, Jian JH, Lu ST, Gao P and Wu XH (2022) Enhanced photocatalytic reduction of carbon dioxide into carbon monoxide by electric field generation and defect engineering in TiO. *Environmental Chemistry Letters* **20**(2), 999–1007.
- Das K, Das R, Riyaz M, Parui A, Bagchi D, Singh AK, Singh AK, Vinod CP and Peter SC (2023) Intrinsic charge polarization in Bi19S27Cl3 Nanorods promotes selective C-C coupling reaction during Photoreduction of CO<sub>2</sub> to ethanol. *Advanced Materials* **35**(5), 2205994.
- Deng BW, Song H, Wang Q, Hong JN, Song S, Zhang YW, Peng K, Zhang HW, Kako T and Ye JH (2023) Highly efficient and stable photothermal catalytic CO<sub>2</sub> hydrogenation to methanol over Ru/In<sub>2</sub>O<sub>3</sub> under atmospheric pressure. *Applied Catalysis B-Environment and Energy* **327**, 122471.
- Deng LL, Sun WZ, Shi ZJ, Qian W, Su Q, Dong L, He HY, Li ZX and Cheng WG (2020) Highly synergistic effect of ionic liquids and Zn-based catalysts for synthesis of cyclic carbonates from urea and diols. *Journal of Molecular Liquids* **316**, 113883.
- Dong TJ, Liu XY, Tang ZF, Yuan HF, Jiang D, Wang YJ, Liu Z, Zhang XL, Huang SF, Liu H, Zhao LL and Zhou WJ (2023) Ru decorated TiO<sub>x</sub> nanoparticles via laser bombardment for photothermal CO-catalytic CO<sub>2</sub> hydrogenation to methane with high selectivity. *Applied Catalysis B-Environment and Energy* **326**, 122176.
- Du C, Wang X, Chen W, Feng S, Wen J and Wu YA (2020) CO<sub>2</sub> transformation to multicarbon products by photocatalysis and electrocatalysis. *Materials Today Advances* **6**, 100071.
- El-Mahdy AFM, Omr HAE, Alothman ZA and Lee H (2023) Design and synthesis of metal-free ethene-based covalent organic framework photocatalysts for efficient, selective, and long-term stable CO<sub>2</sub> conversion into methane. *Journal of Colloid and Interface Science* **633**, 775–785.
- Fang SY, Rahaman M, Bharti J, Reisner E, Robert M, Ozin GA and Hu YH (2023) Photocatalytic CO<sub>2</sub> reduction. *Nature Reviews Methods Primers* **3**(1).
- Feng K, Wang S, Zhang D, Wang L, Yu Y, Feng K, Li Z, Zhu Z, Li C, Cai M, Wu Z, Kong N, Yan B, Zhong J, Zhang X, Ozin GA and He L (2020) Cobalt Plasmonic superstructures enable almost 100% broadband photon efficient CO<sub>2</sub> Photocatalysis. *Advanced Materials* **32**, 2000014.
- Fiorani G and Selva M (2014) Synthesis of dibenzyl carbonate: Towards a sustainable catalytic approach. *RSC Advances* **4**(4), 1929–1937.
- Fu Y, Zhu X, Huang L, Zhang X, Zhang F and Zhu W (2018) Azine-based covalent organic frameworks as metal-free visible light photocatalysts for CO<sub>2</sub> reduction with H<sub>2</sub>O. *Applied Catalysis B: Environmental* **239**, 46–51.
- Gao WL, Liang SY, Wang RJ, Jiang Q, Zhang Y, Zheng QW, Xie BQ, Toe CY, Zhu XC, Wang JY, Huang L, Gao YS, Wang Z, Jo C, Wang Q, Wang LD, Liu YF, Louis B, Scott J, Roger AC, Amal R, Heh H and Park SE (2020) Industrial carbon dioxide capture and utilization: State of the art and future challenges. *Chemical Society Reviews* **49**(23), 8584–8686.
- Gao G, Zhu Z, Zheng J, Liu Z, Wang Q and Yan Y (2019) Ultrathin magnetic Mg-Al LDH photocatalyst for enhanced CO<sub>2</sub> reduction: Fabrication and mechanism. *Journal of Colloid and Interface Science* **555**, 1–10.
- Gong WB, Ye RP, Ding J, Wang TT, Shi XF, Russell CK, Tang JK, Eddings EG, Zhang YL and Fan MH (2020) Effect of copper on highly effective Fe-Mn based catalysts during production of light olefins via Fischer-Tropsch process with low CO<sub>2</sub> emission. *Applied Catalysis B-Environmental* **278**, 119302.
- Gu Y, Tamura M, Nakagawa Y, Ando E and Tomishige K (2023) Effect of flue gas impurities in carbon dioxide from power plants in the synthesis of isopropyl N-phenylcarbamate from CO<sub>2</sub>, aniline, and 2-propanol using CeO<sub>2</sub> and 2-cyanopyridine. *Catalysis Today* **410**, 19–35.
- Guan XS, Jin SB, Liu L, Zhao XY, Zhang XC, Zhang CM, Li Z and Fan CM (2024) Surface engineering of Ce<sub>x</sub>Bi<sub>1-x</sub>O<sub>2-δ</sub> nanorods rich in oxygen vacancies for enhancing photo-thermal synthesis of dimethyl carbonate from CO<sub>2</sub>/CH<sub>3</sub>OH. *Fuel* **358**, 130215.
- Guo C, Tang YX, Yang ZY, Zhao TT, Liu JR, Zhao YF and Wang FL (2023) Reinforcing the efficiency of Photothermal catalytic CO<sub>2</sub> Methanation through integration of Ru nanoparticles with Photothermal MnCo<sub>2</sub>O<sub>4</sub> Nanosheets. *ACS Nano* **17**(23), 23761–23771.
- Guo C, Wang LG, Tang YX, Yang ZY, Zhao YF, Jiang YY, Wen XD and Wang FL (2025) Enhanced photo-thermal CO<sub>2</sub> Methanation with Tunable Ru<sub>x</sub>Ni<sub>1-x</sub> catalytic sites: Alloying beyond pure Ru. *Advanced Functional Materials* **35**(6).
- He X, Gao X, Chen X, Hu S, Tan F, Xiong Y, Long R, Liu M, Tse ECM, Wei F, Yang H, Hou J, Song C and Guo X (2023) Dual-optimization strategy engineered Ti-based metal-organic framework with Fe active sites for highly-selective CO<sub>2</sub> photoreduction to formic acid. *Applied Catalysis B: Environmental* **327**, 122418.
- He YM, Liu SL, Fu WJ, Chen J, Zhai YP, Bi XX, Ren J, Sun RY, Tang ZC, Mebrahtu C and Zeng F (2023) Assessing the efficiency of CO<sub>2</sub> hydrogenation for emission reduction: Simulating ethanol synthesis process as a case study. *Chemical Engineering Research & Design* **195**, 106–115.
- Hu CC, Yoshida M, Chen HC, Tsunekawa S, Lin YF and Huang JH (2021) Production of glycerol carbonate from carboxylation of glycerol with CO<sub>2</sub> using ZIF-67 as a catalyst. *Chemical Engineering Science* **235**, 116451.
- Hu H, Zhang RY, Wang JG, Ying WB and Zhu J (2018) Synthesis and structure-property relationship of biobased biodegradable poly(butylene carbonate-co-furandicarboxylate). *ACS Sustainable Chemistry & Engineering* **6**(6), 7488–7498.

- Huang TH, Chen YS and Yu BY (2023) Techno-economic, environmental, and exergetic evaluation of a novel isopropyl n-phenylcarbamate production process through non-reductive conversion of CO<sub>2</sub>. *Process Saf Environ* **179**, 124–136.
- Huang J-R, Shi W-X, Xu S-Y, Luo H, Zhang J, Lu T-B and Zhang Z-M (2024) Water-mediated selectivity control of CH<sub>3</sub>OH versus CO/CH<sub>4</sub> in CO<sub>2</sub> Photoreduction on single-atom implanted nanotube arrays. *Advanced Materials* **36**(9), 2306906.
- Huang Z, Sun S, Ma M, Liu Y, Zhong X, Chen J, Gao F, Hai G and Huang X (2025) Facile synthesis of TiO<sub>2</sub> supported Pd nanoparticles for efficient photocatalytic CO<sub>2</sub> reduction to CH<sub>4</sub> with H<sub>2</sub>O. *Sustainable Materials and Technologies* **43**, e01247.
- Huang TW and Yu BY (2025) Technological assessment of glycerol carbonate (GC) synthesis via direct conversion of carbon dioxide: An examination of process design, techno-economic analysis, life cycle assessment, and safety evaluation. *Process Safety and Environmental Protection* **201**, 107485.
- Hwang Y, Sorcar S, Lee J, Jung J, Cho C and In S-i (2023) Reduced TiO<sub>2</sub> quantum dots/graphene for solar light driven CO<sub>2</sub> reduction into precisely controlled C<sub>1</sub> vs C<sub>2</sub> hydrocarbon products without noble CO-catalyst. *Journal of Power Sources* **556**, 232430.
- Jesic D, Jurkovic DL, Pohar A, Suhadolnik L and Likozar B (2021) Engineering photocatalytic and photoelectrocatalytic CO<sub>2</sub> reduction reactions: Mechanisms, intrinsic kinetics, mass transfer resistances, reactors and multi-scale modelling simulations. *Chemical Engineering Journal* **407**, 126799.
- Jhuang LJ, Yang CJ and Yu BY (2025) Exploration of alternative reactor configurations for the Fischer-Tropsch (FT) reaction via direct hydrogenation of carbon dioxide. *Journal of the Taiwan Institute of Chemical Engineers* **169**, 105989.
- Ji J, Li R, Zhang H, Duan Y, Liu Q, Wang H and Shen Z (2023) Highly selective photocatalytic reduction of CO<sub>2</sub> to ethane over au-O-Ce sites at micro-interface. *Applied Catalysis B: Environmental* **321**, 122020.
- Jia J, Luo Y, Wu H, Wang Y, Jia X, Wan J, Dang Y, Liu G, Xie H and Zhang Y (2024) Nickel selenide/g-C<sub>3</sub>N<sub>4</sub> heterojunction photocatalyst promotes C-C coupling for photocatalytic CO<sub>2</sub> reduction to ethane. *Journal of Colloid and Interface Science* **658**, 966–975.
- Jiang ZY, Zhao SY, Yang YH, Tan MH, Yang GH and Tan YS (2023) Direct synthesis of dimethyl carbonate from carbon dioxide and methanol over Ce-BTC-derived CeO<sub>2</sub>. *Chemical Engineering Science* **275**, 118760.
- Jin SB, Guan XS, Zhang XC, Zhang CM, Liu JX, Wang YW, Wang YF, Li R, Li Z and Fan CM (2023) CeO<sub>2</sub> nanorods with bifunctional oxygen vacancies for promoting low-pressure photothermocatalytic CO<sub>2</sub> conversion with CH<sub>3</sub>OH to dimethyl carbonate. *Journal of Environmental Chemical Engineering* **11**(6).
- Kou J, Lu C, Wang J, Chen Y, Xu Z and Varma RS (2017) Selectivity enhancement in heterogeneous photocatalytic transformations. *Chemical Reviews* **117**(3), 1445–1514.
- Kovacic Z, Likozar B and Hus M (2020) Photocatalytic CO<sub>2</sub> reduction: A review of ab initio mechanism, kinetics, and multiscale Modeling simulations. *ACS Catalysis* **10**(24), 14984–15007.
- Kuang P, Low J, Cheng B, Yu J and Fan J (2020) MXene-based photocatalysts. *Journal of Materials Science & Technology* **56**, 18–44.
- Kumar S, Hassan I, Regue M, Gonzalez-Carrero S, Rattner E, Isaacs MA and Eslava S (2021) Mechanochemically synthesized Pb-free halide perovskite-based Cs<sub>2</sub>AgBiBr<sub>6</sub>-cu-RGO nanocomposite for photocatalytic CO<sub>2</sub> reduction. *Journal of Materials Chemistry A* **9**(20), 12179–12187.
- Kumar P, Singh G, Guan XW, Lee J, Bahadur R, Ramadass K, Kumar P, Kibria MG, Vidyasagar D, Yi JB and Vinu A (2023) Multifunctional carbon nitride nanoarchitectures for catalysis. *Chemical Society Reviews* **52**(21), 7602–7664.
- Lage VD, Le Valant A, Bion N and Toniolo FS (2023) Tuning co-cu-Al catalysts and their reaction conditions on the CO<sub>2</sub> hydrogenation reaction to higher alcohols under mild conditions. *Chemical Engineering Science* **281**, 119280.
- Lee MT, Chiu HH and Yu BY (2025) Exploration of environmentally friendly processes for converting CO<sub>2</sub> into propanol through direct hydrogenation. *Journal of Industrial and Engineering Chemistry* **143**, 271–282.
- Lee D-E, Kim DJ, Moru S, Kim MG, Jo W-K and Tonda S (2021) Highly-configured TiO<sub>2</sub> hollow spheres adorned with N-doped carbon dots as a high-performance photocatalyst for solar-induced CO<sub>2</sub> reduction to methane. *Applied Surface Science* **563**, 150292.
- Lee CT, Tsai CC, Wu PJ, Yu BY and Lin ST (2021) Screening of CO<sub>2</sub> utilization routes from process simulation: Design, optimization, environmental and techno-economic analysis. *Journal of CO<sub>2</sub> Utilization* **53**, 101722.
- Li H, Guo C, Guo H, Yu C, Li X and Gao X (2019) Methodology for design of vapor permeation membrane-assisted distillation processes for aqueous azeotrope dehydration. *Journal of Membrane Science* **579**, 318–328.
- Li YJ, Liu HM, Ma L, Liu JX and He DH (2021) Transforming glycerol and CO<sub>2</sub> into glycerol carbonate over La<sub>2</sub>O<sub>3</sub>-CO<sub>3</sub>-ZnO catalyst - a case study of the photo-thermal synergism. *Catalysis Science & Technology* **11**(3), 1007–1013.
- Li Y, Liu H, Ma L, Liu J and He D (2024) Photothermal synthesis of glycerol carbonate via glycerol carbonylation with CO<sub>2</sub> over au/Co<sub>3</sub>O<sub>4</sub>-ZnO catalyst. *Acta Physico-Chimica Sinica* **40**(9), 2308005.
- Li N, Liu X, Zhou J, Chen W and Liu M (2020) Encapsulating CuO quantum dots in MIL-125(Ti) coupled with g-C<sub>3</sub>N<sub>4</sub> for efficient photocatalytic CO<sub>2</sub> reduction. *Chemical Engineering Journal* **399**, 125782.
- Li YG, Meng FQ, Wu QX, Yuan DC, Wang HX, Liu B, Wang JW, San XY, Gu L and Meng QB (2024) A Ni-O-ag photothermal catalyst enables 103-m artificial photosynthesis with >17% solar-to-chemical energy conversion efficiency. *Science Advances* **10**(20).
- Li Q, Song T, Zhang Y, Wang Q and Yang Y (2021) Boosting photocatalytic activity and stability of Lead-free Cs<sub>3</sub>Bi<sub>2</sub>Br<sub>9</sub> perovskite nanocrystals via In situ growth on monolayer 2D Ti<sub>3</sub>C<sub>2</sub>T<sub>x</sub> MXene for C-H bond oxidation. *ACS Applied Materials & Interfaces* **13**(23), 27323–27333.
- Li SM, Wang CH, Li DS, Xing YM, Zhang XT and Liu YC (2022) Bi<sub>4</sub>TaO<sub>8</sub>Cl/Bi heterojunction enables high-selectivity photothermal catalytic conversion of CO<sub>2</sub>-H<sub>2</sub>O flow to liquid alcohol. *Chemical Engineering Journal* **435**, 135133.
- Li Y, Wei Y, Xiong J, Tang Z, Wang Y, Wang X, Zhao Z and Liu J (2024) Au@ZnS core-shell nanoparticles decorated 3D hierarchical porous TiO<sub>2</sub> photocatalysts for visible-light-driven CO<sub>2</sub> reduction into CH<sub>4</sub>. *Chemical Engineering Science* **292**, 120017.
- Li X, Yu J and Jaroniec M (2016) Hierarchical photocatalysts. *Chemical Society Reviews* **45**(9), 2603–2636.
- Li X, Yu J, Low J, Fang Y, Xiao J and Chen X (2015) Engineering heterogeneous semiconductors for solar water splitting. *Journal of Materials Chemistry A* **3**(6), 2485–2534.
- Liang S, Chen Y, Han W, Jiao Y, Li W and Tian G (2023) Hierarchical S-scheme titanium dioxide@cobalt-nickel based metal-organic framework nanotube photocatalyst for selective carbon dioxide photoreduction to methane. *Journal of Colloid and Interface Science* **630**, 11–22.
- Liang Y, Wu X, Liu X, Li C and Liu S (2022) Recovering solar fuels from photocatalytic CO<sub>2</sub> reduction over W<sup>6+</sup>-incorporated crystalline g-C<sub>3</sub>N<sub>4</sub> nanorods by synergetic modulation of active centers. *Applied Catalysis B: Environmental* **304**, 120978.
- Liang J, Yu H, Shi J, Li B, Wu L and Wang M (2023) Dislocated bilayer MOF enables high-selectivity photocatalytic reduction of CO<sub>2</sub> to CO. *Advanced Materials* **35**(10), 2209814.
- Liao YL, Wang ZT, Li JH, Fan YJ, Wang DV, Shi L and Lin WB (2024) Bifunctional metal-organic layer for selective photocatalytic carbon dioxide reduction to carbon monoxide. *ACS Catalysis* **14**(22), 16957–16962.
- Lin LL, Gerlak CA, Liu C, Llorca J, Yao SY, Rui N, Zhang F, Liu ZY, Zhang S, Deng KX, Murray CB, Rodriguez JA and Senanayake SD (2021) Effect of Ni particle size on the production of renewable methane from CO<sub>2</sub> over Ni/CeO<sub>2</sub> catalyst. *Journal of Energy Chemistry* **61**, 602–611.
- Lin JX, Wang WJ, Yu BY, Ong CW and Chen CL (2024) Intensification of the CO<sub>2</sub>-capturing methanol steam reforming process: A comprehensive analysis of energy, economic and environmental impacts. *Separation and Purification Technology* **347**, 127612.
- Liu P, Chen H, Zhao C, Long D, Chen W, Lu M and Chen X (2024) A quadruple transition metal dichalcogenide for variously synergetic electron behaviors during photocatalytic carbon dioxide reduction. *Applied Surface Science* **659**, 159887.
- Liu JX, Li YJ, Liu HM and He DH (2019) Photo-thermal synergistically catalytic conversion of glycerol and carbon dioxide to glycerol carbonate over au/ZnWO<sub>4</sub>-ZnO catalysts. *Applied Catalysis B-Environmental* **244**, 836–843.
- Liu HM, Li YJ, Ma L, Liu JX and He DH (2022) Photo-thermal conversion of CO<sub>2</sub> and biomass-based glycerol into glycerol carbonate over Co<sub>3</sub>O<sub>4</sub>-ZnO p-n heterojunction catalysts. *Fuel* **315**, 123294.



- Liu HX, Li SQ, Wang WW, Yu WZ, Zhang WJ, Ma C and Jia CJ (2022) Partially sintered copper-ceria as excellent catalyst for the high-temperature reverse water gas shift reaction. *Nature Communications* 13(1).
- Liu G, Yang G, Peng X, Wu J and Tsubaki N (2022) Recent advances in the routes and catalysts for ethanol synthesis from syngas. *Chemical Society Reviews* 51(13), 5606–5659.
- Lou Y, Jiang F, Zhu W, Wang L, Yao TY, Wang SS, Yang B, Yang B, Zhu YF and Liu XH (2021) CeO<sub>2</sub> supported Pd dimers boosting CO<sub>2</sub> hydrogenation to ethanol. *Applied Catalysis B-Environmental*, 291, 120122.
- Lu C, Li J, Yan J, Li B, Huang B and Lou Z (2020) Surface plasmon resonance and defects on tungsten oxides synergistically boost high-selective CO<sub>2</sub> reduction for ethylene. *Applied Materials Today* 20, 100744.
- Lu XS, Luo XJ, Tan JZY and Maroto-Valer M (2021) Simulation of CO<sub>2</sub> photoreduction in a twin reactor by multiphysics models. *Chemical Engineering Research & Design* 171, 125–138.
- Luo C, Tang HR, Lu HF, Wu KJ, Liu YY, Zhu YM, Wang BS and Liang B (2024) Construction of DBU-based poly (ionic liquid)s for the conversion of CO<sub>2</sub>, glycerol, and propylene oxide into glycerol carbonate. *ChemCatChem* 16(12).
- Ma QX, Zhao TS, Wang D, Niu WQ, Lv P and Tsubaki N (2013) Synthesis of dipropyl carbonate over calcined hydrotalcite-like compounds containing La. *Applied Catalysis a-General* 464, 142–148.
- Madi MO and Tahir M (2024) Well-designed 2D vanadium carbide (V<sub>2</sub>C) MXenes supported LaCoO<sub>3</sub>/g-C<sub>3</sub>N<sub>4</sub> heterojunction for highly efficient and stable photocatalytic CO<sub>2</sub> reduction to CO and CH<sub>4</sub>. *Journal of Alloys and Compounds* 983, 173730.
- Mahmoudkhani M and Keith DW (2009) Low-energy sodium hydroxide recovery for CO<sub>2</sub> capture from atmospheric air—Thermodynamic analysis. *International Journal of Greenhouse Gas Control* 3(4), 376–384.
- Man S, Jiang W, Guo X, Ruzimuradov O, Mamatkulov S, Low J and Xiong Y (2024) Materials Design for Photocatalytic CO<sub>2</sub> conversion to C<sub>2+</sub> products. *Chemistry of Materials* 36(4), 1793–1809.
- Manna R, Bhattacharya G, Raj S and Samanta AN (2024) Boosting photocatalytic CO<sub>2</sub> reduction efficiency by graphene nanoflakes (GNF) decorated ZIF-67 under visible light irradiation. *Journal of Environmental Chemical Engineering* 12(1), 111722.
- Meesattham S and Kim-Lohsoontorn P (2022) Low-temperature alcohol-assisted methanol synthesis from CO<sub>2</sub> and H<sub>2</sub>: The effect of alcohol type. *International Journal of Hydrogen Energy* 47(54), 22691–22703.
- More GS and Srivastava R (2021) Efficient activation of CO<sub>2</sub> over Ce-MOF-derived CeO<sub>2</sub> for the synthesis of cyclic urea, urethane, and carbamate. *Industrial and Engineering Chemistry Research* 60(34), 12492–12504.
- Mori K, Konishi A and Yamashita H (2020) Interfacial engineering of PdAg/TiO<sub>2</sub> with a metal-organic framework to promote the hydrogenation of CO<sub>2</sub> to formic acid. *Journal of Physical Chemistry C* 124(21), 11499–11505.
- Ning SB, Wang JW, Wu XT, Li L, Zhang SL, Chen SH, Ren XH, Gao LJ, Hao YC, Lv CC, Li YG and Ye JH (2024) Natural sunlight-driven CO<sub>2</sub> hydrogenation into light olefins at ambient pressure over Bifunctional Cu-promoted CoFe alloy catalyst. *Advanced Functional Materials* 34(30).
- OConnell GEP, Tan TH, Yuwono JA, Wang Y, Kheradmand A, Jiang YJ, Kumar P, Amal R, Scott J and Lovell EC (2024) Seeing the light: The role of cobalt in light-assisted CO<sub>2</sub> methanation. *Applied Catalysis B-Environment and Energy* 343, 123507.
- Omr HAE, Putikam R, Hussien MK, Sabbah A, Lin T-Y, Chen K-H, Wu H-L, Feng S-P, Lin M-C and Lee H (2023) Design of sculptured SnS/g-C<sub>3</sub>N<sub>4</sub> photocatalytic nanostructure for highly efficient and selective CO<sub>2</sub> conversion to methane. *Applied Catalysis B: Environmental* 324, 122231.
- Onishi N and Himeda Y (2022) Homogeneous catalysts for CO<sub>2</sub> hydrogenation to methanol and methanol dehydrogenation to hydrogen generation. *Coordination Chemistry Reviews* 472, 214767.
- Pérez-Fortes M, Schöneberger JC, Boulamanti A, Harrison G and Tzimas E (2016) Formic acid synthesis using CO<sub>2</sub> as raw material: Techno-economic and environmental evaluation and market potential. *International Journal of Hydrogen Energy* 41(37), 16444–16462.
- Putro WS, Ijima S, Matsumoto S, Hamura S, Yabushita M, Tomishige K, Fukaya N and Choi JC (2024) Sustainable synthesis of diethyl carbonate from carbon dioxide and ethanol featuring acetals as regenerable dehydrating agents. *RSC Sustainability* 2(5), 1613–1620.
- Putro WS, Munakata Y, Ijima S, Shigeyasu S, Hamura S, Matsumoto S, Mishima T, Tomishige K, Choi JC and Fukaya N (2022) Synthesis of diethyl carbonate from CO<sub>2</sub> and orthoester promoted by a CeO<sub>2</sub> catalyst and ethanol. *Journal of CO<sub>2</sub> Utilization* 55, 101818.
- Quilis C, Mota N, Pawelec B, Millan E and Yerga RMN (2023) Intermetallic PdZn/TiO<sub>2</sub> catalysts for methanol production from CO<sub>2</sub> hydrogenation: The effect of ZnO loading on PdZn-ZnO sites and its influence on activity. *Applied Catalysis B: Environmental* 321, 122064.
- Ramezani SF, Karimi M, Panahi M and Rafiee A (2020) Sustainable dimethyl carbonate production from ethylene oxide and methanol. *Chemical Engineering & Technology* 43(12), 2484–2492.
- Ramyashree MS, Nandy A, Bohari YR, Pramodh M, Kumar SH, Priya SS and Sudhakar K (2024) Modeling and simulation of reactors for methanol production by CO<sub>2</sub> reduction: A comparative study. *Results in Engineering* 23, 102306.
- Rastgaran A, Fatoorehchi H, Khallaghi N, Larimi A and Borhani TN (2023) Modelling of photocatalytic CO<sub>2</sub> reduction into value-added products in a packed bed photoreactor using the ray tracing method. *Carbon Capture Science & Technology* 8, 100118.
- Ray AK (1999) Design, modelling and experimentation of a new large-scale photocatalytic reactor for water treatment. *Chemical Engineering Science* 54(15–16), 3113–3125.
- Ren SY, Han JN, Yang ZW, Liang J, Feng SJ, Zhang X, Xu J and Zhu J (2025) Near-Unity Photothermal CO<sub>2</sub> hydrogenation to methanol based on a molecule/Nanocarbon hybrid catalyst. *Angewandte Chemie-International Edition* 64(4).
- Ren YQ, Si YT, Du MY, You CJ, Zhang CY, Zhu YH, Sun ZK, Huang K, Liu MC, Duan LB and Li NX (2024) Photothermal synergistic effect induces bimetallic cooperation to modulate product selectivity of CO<sub>2</sub> reduction on different CeO<sub>2</sub> crystal facets. *Angewandte Chemie-International Edition* 63(46).
- S.S GC, Alkanad K, T B, Alnaggar G, Al Zaqri N, Drmash QA, Boshala A and L NK (2022) Alkaline mediated sono-synthesis of surface oxygen-vacancies-rich cerium oxide for efficient photocatalytic CO<sub>2</sub> reduction to methanol. *Surfaces and Interfaces* 34, 102389.
- Saadh MJ, Mustafa MA, Altalbawy FMA, Ballal S, Prasad GVS, Al-saray MJ, Abbas JK, Al-Maliky MA, Mohammed Sk, Alam MM and Elawady A (2025) Integration TiO<sub>2</sub> nanosheets into defect engineered Zr-based MOF for highly selective and efficient photocatalytic conversion of CO<sub>2</sub> to ethane. *Journal of Molecular Structure* 1325, 140830.
- Sabatino F, Gazzani M, Gallucci F and van Sint Annaland M (2022) Modeling, optimization, and techno-economic analysis of bipolar membrane electro-dialysis for direct air capture processes. *Industrial and Engineering Chemistry Research* 61(34), 12668–12679.
- Sadanandan AM, Yang JH, Devtade V, Singh G, Dharmarajan NP, Fawaz M, Leec JM, Tavakkoli E, Jeon CH, Kumar P and Vinu A (2024) Carbon nitride based nanoarchitectonics for nature-inspired photocatalytic CO<sub>2</sub> reduction. *Progress in Materials Science* 142, 101242.
- Sahoo RC, Lu H, Garg D, Yin Z and Matte HSSR (2022) Bandgap engineered g-C<sub>3</sub>N<sub>4</sub> and its graphene composites for stable photoreduction of CO<sub>2</sub> to methanol. *Carbon* 192, 101–108.
- Si YT, Li Y, Cheng M, Ren YQ, Zhou JC, Sun ZK, Guan J, Liu MC, Duan LB and Li NX (2025) Synergistic dual-oxygen-vacancy design boosts photothermal CO<sub>2</sub> reduction into ethylene. *Nano Energy*, 138.
- Song W, Wang C, Liu Y, Chong KC, Zhang X, Wang T, Zhang Y, Li B, Tian J, Zhang X, Wang X, Yao B, Wang X, Xiao Y, Yao Y, Mao X, He Q, Lin Z, Zou Z and Liu B (2024) Unlocking copper-free interfacial asymmetric C–C coupling for ethylene photosynthesis from CO<sub>2</sub> and H<sub>2</sub>O. *Journal of the American Chemical Society* 146(42), 29028–29039.
- Summa P, Samojeden B, Motak M, Wierzbicki D, Alneit I, Swierczek K and Da Costa P (2022) Investigation of Cu promotion effect on hydrotalcite-based nickel catalyst for CO<sub>2</sub> methanation. *Catalysis Today* 384, 133–145.
- Tahir M and Tahir B (2020) 2D/2D/2D O-C<sub>3</sub>N<sub>4</sub>/Bt/Ti<sub>3</sub>C<sub>2</sub>T<sub>x</sub> heterojunction with novel MXene/clay multi-electron mediator for stimulating photo-induced CO<sub>2</sub> reforming to CO and CH<sub>4</sub>. *Chemical Engineering Journal* 400, 125868.
- Tan L, Xu S-M, Wang Z, Xu Y, Wang X, Hao X, Bai S, Ning C, Wang Y, Zhang W, Jo YK, Hwang S-J, Cao X, Zheng X, Yan H, Zhao Y, Duan H and Song Y-F (2019) Highly selective Photoreduction of CO<sub>2</sub> with suppressing H<sub>2</sub>

- evolution over monolayer layered double hydroxide under irradiation above 600 nm. *Angewandte Chemie International Edition* **58**(34), 11860–11867.
- Tang YX, Wang H, Guo C, Wang LG, Zhao TT, Xiao SK, Liu JR, Jiang YY, Zhao YF, Wen XD and Wang FL (2025) Synergies between atomically dispersed Ru single atoms and nanoparticles on CeAlOx for enhanced photo-thermal catalytic CO<sub>2</sub> hydrogenation. *Advanced Materials* e12793.
- Tang YX, Wang H, Guo C, Wang LG, Zhao TT, Yang ZY, Xiao SK, Liu JR, Jiang YY, Zhao YF, Wen XD and Wang FL (2024) F-coordinated single-atom Ru species: Efficient and durable catalysts for photo-thermal synergistic catalytic CO<sub>2</sub> hydrogenation to methane. *Journal of Materials Chemistry A* **12**(32), 20958–20966.
- Tang YX, Wang H, Guo C, Yang ZY, Zhao TT, Liu JR, Jiang YY, Wang WL, Zhang Q, Wu DS, Zhao YF, Wen XD and Wang FL (2024) Ruthenium-cobalt solid-solution alloy nanoparticles for enhanced Photopromoted Thermocatalytic CO<sub>2</sub> hydrogenation to methane. *ACS Nano* **18**(17), 11449–11461.
- Tomishige K, Gu Y, Nakagawa Y and Tamura M (2020) Reaction of CO<sub>2</sub> with alcohols to linear-, cyclic-, and poly-carbonates using CeO<sub>2</sub>-based catalysts. *Frontiers in Energy Research*, 8.
- Tomishige K, Tamura M and Nakagawa Y (2019) CO<sub>2</sub> conversion with alcohols and amines into carbonates, Ureas, and carbamates over CeO<sub>2</sub> catalyst in the presence and absence of 2-Cyanopyridine. *Chemical Record* **19**(7), 1354–1379.
- Tu Z, Lu Y, Liu LP, Wang LZ, Li Y and Wei ZY (2023) Modification of biodegradable poly(butylene carbonate) by biobased cis-2-butene-1,4-diol. *European Polymer Journal*, 198.
- Uddin Z, Yu BY and Lee HY (2022) Evaluation of alternative processes of CO<sub>2</sub> methanation: Design, optimization, control, techno-economic and environmental analysis. *J Co2 Util*, 60.
- Vahidzadeh E, Zeng S, Manuel AP, Riddell S, Kumar P, Alam KM and Shankar K (2021) Asymmetric multipole Plasmon-mediated catalysis shifts the product selectivity of CO<sub>2</sub> Photoreduction toward C<sub>2+</sub> products. *ACS Applied Materials & Interfaces* **13**(6), 7248–7258.
- Variar AG, Ramyashree MS, Ail VU, Priya SS, Sudhakar K and Tahir M (2021) Influence of various operational parameters in enhancing photocatalytic reduction efficiency of carbon dioxide in a photoreactor: A review. *Journal of Industrial and Engineering Chemistry* **99**, 19–47.
- Vennapoosa CS, Tejavath V, Prabhu YT, Tiwari A, Abraham BM, Upadhyayula VS and Pal U (2023) Sulphur vacancy-rich PCdS/NiCoLDH promotes highly selective and efficient photocatalytic CO<sub>2</sub> reduction to MeOH. *J Co2 Util* **67**, 102332.
- Vo CH, Pérez-Ramírez J, Farooq S and Karimi IA (2022) *Prospects of Producing Higher Alcohols from Carbon Dioxide: A Process System Engineering Perspective*. *Acs Sustainable Chemistry & Engineering*
- Wang HL, Bootharaju MS, Kim JH, Wang Y, Wang K, Zhao M, Zhang R, Xu J, Hyeon T, Wang X, Song SY and Zhang HJ (2023) Synergistic interactions of Neighboring platinum and iron atoms enhance reverse water-gas shift reaction performance. *Journal of the American Chemical Society*.
- Wang Q, Chen Y, Liu X, Li L, Du L and Tian G (2021) Sulfur doped In<sub>2</sub>O<sub>3</sub>-CeO<sub>2</sub> hollow hexagonal prisms with carbon coating for efficient photocatalytic CO<sub>2</sub> reduction. *Chemical Engineering Journal* **421**, 129968.
- Wang G, Chen Z, Wang T, Wang D and Mao J (2022) P and cu dual sites on graphitic carbon nitride for photocatalytic CO<sub>2</sub> reduction to hydrocarbon fuels with high C<sub>2</sub>H<sub>6</sub> evolution. *Angewandte Chemie International Edition* **61**(40), e202210789.
- Wang H, Cheng S, Cai X, Cheng L, Zhou R, Hou T and Li Y (2022) Photocatalytic CO<sub>2</sub> reduction to HCOOH over core-shell Cu@Cu<sub>2</sub>O catalysts. *Catalysis Communications* **162**, 106372.
- Wang K, Cheng M, Wang N, Zhang Q, Liu Y, Liang J, Guan J, Liu M, Zhou J and Li N (2023) Inter-plane 2D/2D ultrathin La<sub>2</sub>Ti<sub>2</sub>O<sub>7</sub>/Ti<sub>3</sub>C<sub>2</sub> MXene Schottky heterojunctions toward high-efficiency photocatalytic CO<sub>2</sub> reduction. *Chinese Journal of Catalysis* **44**, 146–159.
- Wang Q, Hu KH, Gao RX, Zhang LY, Wang L and Zhang CD (2022) Hydrogenation of carbon dioxide to value-added liquid fuels and aromatics over Fe-based catalysts based on the Fischer-Tropsch synthesis route. *Atmosphere* **13**(8).
- Wang K, Li X, Wang N, Shen Q, Liu M, Zhou J and Li N (2021) Z-scheme Core-Shell meso-TiO<sub>2</sub>@ZnIn<sub>2</sub>S<sub>4</sub>/Ti<sub>3</sub>C<sub>2</sub> MXene enhances visible light-driven CO<sub>2</sub>-to-CH<sub>4</sub> selectivity. *Industrial and Engineering Chemistry Research* **60**(24), 8720–8732.
- Wang C, Liu L, Li H, Wang L and Xiao F-S (2023) Hydrophobic catalysts for syngas conversion. *Matter* **6**(9), 2697–2710.
- Wang PX, Liu SM, Zhou F, Yang BQ, Alshammari AS, Lu LJ and Deng YQ (2014) Two-step synthesis of dimethyl carbonate from urea, ethylene glycol and methanol using acid-base bifunctional zinc-yttrium oxides. *Fuel Processing Technology* **126**, 359–365.
- Wang K, Lu J, Lu Y, Lau CH, Zheng Y and Fan X (2021) Unravelling the C-C coupling in CO<sub>2</sub> photocatalytic reduction with H<sub>2</sub>O on Au/TiO<sub>2-x</sub>: Combination of plasmonic excitation and oxygen vacancy. *Applied Catalysis B: Environmental* **292**, 120147.
- Wang XL, Ramirez PJ, Liao WJ, Rodriguez JA and Liu P (2021) Cesium-induced active sites for C-C coupling and ethanol synthesis from CO<sub>2</sub> hydrogenation on Cu/ZnO(0001) surfaces. *Journal of the American Chemical Society* **143**(33), 13103–13112.
- Wang K, Wang Q, Zhang K, Wang G and Wang H (2022) Selective solar-driven CO<sub>2</sub> reduction mediated by 2D/2D Bi<sub>2</sub>O<sub>3</sub>/SiO<sub>3</sub>/MXene nanosheets heterojunction. *Journal of Materials Science & Technology* **124**, 202–208.
- Wang Y, Zhang Z, Zhang L, Luo Z, Shen J, Lin H, Long J, Wu JCS, Fu X, Wang X and Li C (2018) Visible-light driven overall conversion of CO<sub>2</sub> and H<sub>2</sub>O to CH<sub>4</sub> and O<sub>2</sub> on 3D-SiC@2D-MoS<sub>2</sub> Heterostructure. *Journal of the American Chemical Society* **140**(44), 14595–14598.
- Wang K, Zhang R, Zhou B, Li Q, Zhou M, Shen H-M, Wang Q, Xia J, Li H, Yi Q and She Y (2025) Highly selective photocatalytic CO<sub>2</sub> reduction into C<sub>2</sub>H<sub>4</sub> enabled by metal-organic framework-derived catalysts with high Cu<sup>+</sup> content. *Journal of Colloid and Interface Science* **677**, 872–881.
- Wang Z, Zhu J, Zu X, Wu Y, Shang S, Ling P, Qiao P, Liu C, Hu J, Pan Y, Zhu J, Sun Y and Xie Y (2022) Selective CO<sub>2</sub> Photoreduction to CH<sub>4</sub> via Pd<sup>6+</sup>-assisted Hydrodeoxygenation over CeO<sub>2</sub> Nanosheets. *Angewandte Chemie International Edition* **61**(30), e202203249.
- Weilhard A, Argent SP and Sans V (2021) Efficient carbon dioxide hydrogenation to formic acid with buffering ionic liquids. *Nature Communications* **12**(1).
- Wen D, Wang N, Peng J, Majima T and Jiang J (2025) Collaborative photocatalytic C-C coupling with Cu and P dual sites to produce C<sub>2</sub>H<sub>4</sub> over Cu<sub>x</sub>P/g-C<sub>3</sub>N<sub>4</sub> heterojunction. *Chinese Journal of Catalysis* **69**, 58–74.
- Wu PJ, Hsu CC, Yu BY and Lin ST (2024) Rigorous simulation and comprehensive analysis for the novel glycerol carbonate (GC) production process via indirect conversion of CO<sub>2</sub>. *Fuel*, 357.
- Wu ZY, Li CR, Li Z, Feng K, Cai MJ, Zhang DK, Wang SH, Chu MY, Zhang CC, Shen JH, Huang Z, Xiao YL, Ozin GA, Zhang XH and He L (2021) Niobium and titanium carbides (MXenes) as superior Photothermal supports for CO<sub>2</sub> Photocatalysis. *ACS Nano* **15**(3), 5696–5705.
- Wu L, Li Y, Zhou B, Liu J, Cheng D, Guo S, Xu K, Yuan C, Wang M, Hong Melvin GJ, Ortiz-Medina J, Ali S, Yang T, Kim YA and Wang Z (2023) Vertical graphene on rice-husk-derived SiC/C composite for highly selective photocatalytic CO<sub>2</sub> reduction into CO. *Carbon* **207**, 36–48.
- Wu QX, Wang JL, Yuan DC, Wang YC, Li YG, Guo YN, Zhang ZB, San XY, Zhang LQ and Ye JH (2025) Ambient sunlight driven Photothermal green syngas production at 100 m<sup>2</sup> scale by the dynamic structural reconstruction of iron oxides with 38.7% efficiency. *Advanced Functional Materials* **35**(2).
- Xi H, Xu Y, Zou W, Ji J, Cai Y, Wan H and Dong L (2022) Enhanced methanol selectivity of Cu<sub>x</sub>O/TiO<sub>2</sub> photocatalytic CO<sub>2</sub> reduction: Synergistic mechanism of surface hydroxyl and low-valence copper species. *J Co2 Util* **55**, 101825.
- Xie S, Li Y, Sheng B, Zhang W, Wang W, Chen C, Li J, Sheng H and Zhao J (2022) Self-reconstruction of paddle-wheel copper-node to facilitate the photocatalytic CO<sub>2</sub> reduction to ethane. *Applied Catalysis B: Environmental* **310**, 121320.
- Xie BQ, Wong RJ, Tan TH, Higham M, Gibson EK, Decarolis D, Callison J, Aguey-Zinsou KF, Bowker M, Catlow CRA, Scott J and Amal R (2020) Synergistic ultraviolet and visible light photo-activation enables intensified low-temperature methanol synthesis over copper/zinc oxide/alumina. *Nature Communications* **11**(1).
- Xu Y.F., Tountas, A.A., Song, R., Ye, J., Wei, J.H., Ji, S.F., Zhao, L., Zhou, W.Z., Chen, J.H., Zhao, G.S., Yao X., Sain M.M., Kuang D.B., Ozin G.A., Yao, X.D., Sain, M.M., Kuang, D.B., Ozin, G.A. Equilibrium photo-thermodynamics enables a sustainable methanol synthesis. *Joule*, 2023. 7(4): p. 738–752.

- Xu Y-F, Yang M-Z, Chen B-X, Wang X-D, Chen H-Y, Kuang D-B and Su C-Y (2017) A CsPbBr<sub>3</sub> perovskite quantum dot/graphene oxide composite for photocatalytic CO<sub>2</sub> reduction. *Journal of the American Chemical Society* **139**(16), 5660–5663.
- Xu F, Zhu B, Cheng B, Yu J and Xu J (2018) 1D/2D TiO<sub>2</sub>/MoS<sub>2</sub> hybrid nanostructures for enhanced photocatalytic CO<sub>2</sub> reduction. *Advanced Optical Materials* **6**(23), 1800911.
- Yabushita M, Fujii R, Nakagawa Y and Tomishige K (2024) Thermodynamic and catalytic insights into non-reductive transformation of CO<sub>2</sub> with amines into organic urea derivatives. *ChemCatChem* **16**(6).
- Yan X, Gao B, Zheng X, Cheng M, Zhou N, Liu X, Du L, Yuan F, Wang J, Cui X, Zhang G, Kong W and Xu Q (2024) Cooperatively tailored surface frustrated Lewis pairs and N-doping on CeO<sub>2</sub> for photocatalytic CO<sub>2</sub> reduction to high-value hydrocarbon products. *Applied Catalysis B: Environmental* **343**, 123484.
- Yan K, Wu DH, Wang T, Chen C, Liu SJ, Hu YG, Gao C, Chen HY and Li BX (2023) Highly selective ethylene production from solar-driven CO<sub>2</sub> reduction on the Bi<sub>2</sub>S<sub>3</sub>@In<sub>2</sub>S<sub>3</sub> catalyst with In-SV-Bi active sites. *ACS Catalysis* **13**(4), 2302–2312.
- Yan B-H, Xu B-R, Jin Y, Xiao H, Luo S-C, Duan R-H, Li H, Yan X-Q, Lin B and Yang G-D (2024) AuAg plasmonic nanoalloys with asymmetric charge distribution on CeO<sub>2</sub> nanorods for selective photocatalytic CO<sub>2</sub>-to-CH<sub>4</sub> conversion. *cMat* **1**(3), e28.
- Yang H, Hou H, Yang M, Zhu Z, Fu H, Zhang D, Luo Y and Yang W (2023) Engineering the S-scheme heterojunction between NiO microrods and MgAl-LDH nanoplates for efficient and selective photoreduction of CO<sub>2</sub> to CH<sub>4</sub>. *Chemical Engineering Journal* **474**, 145813.
- Yang Y-N, Huang C-W, Nguyen V-H and Wu JCS (2022) Enhanced methanol production by two-stage reaction of CO<sub>2</sub> hydrogenation at atmospheric pressure. *Catalysis Communications* **162**, 106373.
- Yang X, Lan X, Zhang Y, Li H and Bai G (2023) Rational design of MoS<sub>2</sub>@COF hybrid composites promoting C-C coupling for photocatalytic CO<sub>2</sub> reduction to ethane. *Applied Catalysis B: Environmental* **325**, 122393.
- Yang S, Zhang W, Pan G, Chen J, Deng J, Chen K, Xie X, Han D, Dai M and Niu L (2023) Photocatalytic co-reduction of N<sub>2</sub> and CO<sub>2</sub> with CeO<sub>2</sub> catalyst for urea synthesis. *Angewandte Chemie International Edition* **62**(43), e202312076.
- Yang J-J, Zhang Y, Xie X-Y, Fang W-H and Cui G (2022) Photocatalytic reduction of carbon dioxide to methane at the Pd-supported TiO<sub>2</sub> Interface: Mechanistic insights from theoretical studies. *ACS Catalysis* **12**(14), 8558–8571.
- Yu BY, Chen MK and Chien IL (2018) Assessment on CO<sub>2</sub> utilization through rigorous simulation: Converting CO<sub>2</sub> to dimethyl carbonate. *Industrial and Engineering Chemistry Research* **57**(2), 639–652.
- Yu H, Sun C, Xuan Y, Zhang K and Chang K (2022) Full solar spectrum driven plasmonic-assisted efficient photocatalytic CO<sub>2</sub> reduction to ethanol. *Chemical Engineering Journal* **430**, 132940.
- Yu YC, Wang TY, Chang LH, Wu PJ, Yu BY and Yu WY (2020) Conceptual design, environmental, and economic evaluation of direct copolymerization process of carbon dioxide and 1,4-butanediol. *J Taiwan Inst Chem E* **116**, 36–42.
- Yu BY, Wu PJ, Tsai CC and Lin ST (2020) Evaluating the direct CO<sub>2</sub> to diethyl carbonate (DEC) process: Rigorous simulation, techno-economical and environmental evaluation. *J Co2 Util*, 41.
- Zeng S, Vahidzadeh E, VanEssen CG, Kar P, Kisslinger R, Goswami A, Zhang Y, Mahdi N, Riddell S, Kobryn AE, Gusarov S, Kumar P and Shankar K (2020) Optical control of selectivity of high rate CO<sub>2</sub> photoreduction via interband- or hot electron Z-scheme reaction pathways in au-TiO<sub>2</sub> plasmonic photonic crystal photocatalyst. *Applied Catalysis B: Environmental* **267**, 118644.
- Zhai JX, Xia ZH, Zhou BW, Wu HH, Xue T, Chen X, Jiao JP, Jia SQ, He MY and Han BX (2024) Photo-thermal coupling to enhance CO<sub>2</sub> hydrogenation toward CH<sub>4</sub> over Ru/MnO/Mn<sub>3</sub>O<sub>4</sub>. *Nature Communications* **15**(1).
- Zhang XY, Dong CR, Yang Y, Hu YJ, Wu LZ, Gu Y, Zhang K and Shen JY (2024) Highly selective photothermal conversion of CO<sub>2</sub> to ethylene using hierarchical boxwood ball-like Weyl semimetal WTe<sub>2</sub> catalysts. *Journal of Materials Chemistry A* **12**(2), 923–931.
- Zhang JQ, Li M, Tan XJ, Shi L, Xie K, Zhao XL, Wang SJ, Zhao SY, Zhang HY, Duan XG, Chen HJ, Zhu YZ, Wu MB, Sun HQ and Wang SB (2023) Confined FeNi alloy nanoparticles in carbon nanotubes for photothermal oxidative dehydrogenation of ethane by carbon dioxide. *Applied Catalysis B-Environment and Energy*, 339.
- Zhang M, Liu Y, Jia P, Feng Y, Fu S, Yang J, Xiong L, Su F, Wu Y and Huang Y (2021) Ag nanoparticle-decorated mesoporous silica as a dual-mode Raman sensing platform for detection of volatile organic compounds. *ACS Applied Nano Materials* **4**(2), 1019–1028.
- Zhang HF, Wang LG, Van Herle J, Marechal F and Desideri U (2021) Techno-economic comparison of 100% renewable urea production processes. *Applied Energy*, 284.
- Zhang S, Xiong W, Long J, Si Y, Xu Y, Yang L, Zou J, Dai W, Luo X and Luo S (2022) High-throughput lateral and basal interface in CeO<sub>2</sub>@-Ti<sub>3</sub>C<sub>2</sub>X: Reverse and synergistic migration of carrier for enhanced photocatalytic CO<sub>2</sub> reduction. *Journal of Colloid and Interface Science* **615**, 716–724.
- Zhang X, Yang Y, Hu Y, Chen Y, Shen J and Tu Y (2024) Enhanced Photothermal catalytic CO<sub>2</sub> reduction to high selective C<sub>2</sub>H<sub>4</sub> by cooperative interaction of oxygen vacancy and WTe<sub>2</sub> semimetal Cocatalyst In situ grown on WO<sub>3</sub> hollow spheres. *ACS Applied Energy Materials* **7**(24), 11859–11872.
- Zhang XY, Yang Y, Hu YJ, Xiong LJ, Wang TY, Li PJ and Shen JY (2024) Photothermal catalytic C-C coupling to ethylene from CO<sub>2</sub> with high efficiency by synergistic cooperation of oxygen vacancy and half-metallic WTe<sub>2</sub>. *Journal of Energy Chemistry* **93**, 547–556.
- Zhao D, Xuan Y, Sun C, Zhang L, Zhu Q and Liu X (2024) Facilitating photocatalytic CO<sub>2</sub> methanation via synergetic feed of photon-induced carriers and reactants over S-scheme BiVO<sub>4</sub>@TiO<sub>2</sub> nanoglass/needle arrays. *Journal of Catalysis* **439**, 115760.
- Zheng Y, Yin X, Jiang Y, Bai J, Tang Y, Shen Y and Zhang M (2019) Nano ag-decorated MoS<sub>2</sub> Nanosheets from 1T to 2H phase conversion for Photocatalytically reducing CO<sub>2</sub> to methanol. *Energy Technology* **7**(11), 1900582.
- Zhou HC, Long JR and Yaghi OM (2012) Introduction to metal–organic frameworks. *Chemical Reviews* **112**(2), 673–674.